

Article

Diagnosis of the Extreme Climate Events of Temperature and Precipitation in Metropolitan Lima during 1965–2013

Lucy Giráldez ^{1,*} , Yamina Silva ² , José L. Flores-Rojas ¹  and Grace Trasmonte ² 

¹ Instituto Geofísico del Perú, Calle Badajoz 169, Urb. Mayorazgo IV Etapa, Ate, Lima 15012, Perú; jflores@igp.gob.pe

² Departamento de Humanidades, Instituto de la Naturaleza, Tierra y Energía (INTE-PUCP), Pontificia Universidad Católica del Perú, Av. Universitaria 1801, San Miguel, Lima 15088, Perú; fysilva@pucp.pe (Y.S.); gtrasmonte3@gmail.com (G.T.)

* Correspondence: lgiraldez@igp.gob.pe; Tel.: +51-990015171

Abstract: The most extreme precipitation event in Metropolitan Lima (ML) occurred on 15 January 1970 (16 mm), this event caused serious damage, and the real vulnerability of this city was evidenced; the population is still not prepared to resist events of this nature. This research describes the local climate variability and extreme climate indices of temperature and precipitation. In addition, the most extreme precipitation event in ML is analyzed. Extreme climate indices were identified based on the methodology proposed by the Expert Team on Climate Change Detection and Indices (ETCCDI). Some extreme temperature indices highlight an initial trend toward warm conditions (1965–1998); this trend has changed towards cold conditions since 1999, consistent with the thermal cooling during the last two decades in ML (-0.5 °C/decade) and other coastal areas of Peru. The variations of extreme temperature indices are mainly modulated by sea-surface temperature (SST) alterations in the Niño 1 + 2 region (moderate to strong correlations were found). Extreme precipitation indices show trends toward wet conditions after the 1980s, the influence of the Pacific Ocean SST on the extreme precipitation indices in ML is weak and variable in sign. The most extreme precipitation event in ML is associated with a convergence process between moisture fluxes from the east (Amazon region) at high and mid levels and moisture fluxes from the west (Pacific Ocean) at low levels, and near the surface.

Keywords: Metropolitan Lima; extreme climate indices; extreme precipitation; warm days; cold days; 15 January 1970



Citation: Giráldez, L.; Silva, Y.; Flores-Rojas, J.L.; Trasmonte, G. Diagnosis of the Extreme Climate Events of Temperature and Precipitation in Metropolitan Lima during 1965–2013. *Climate* **2022**, *10*, 112. <https://doi.org/10.3390/cli10080112>

Academic Editors: Oeurng Chantha, Try Sophal and Sok Ty

Received: 4 May 2022
Accepted: 20 July 2022
Published: 23 July 2022

Publisher's Note: MDPI stays neutral with regard to jurisdictional claims in published maps and institutional affiliations.



Copyright: © 2022 by the authors. Licensee MDPI, Basel, Switzerland. This article is an open access article distributed under the terms and conditions of the Creative Commons Attribution (CC BY) license (<https://creativecommons.org/licenses/by/4.0/>).

1. Introduction

Lima, the capital of Peru, is the largest and most populous city in the country and one of the most overpopulated cities in Latin America. The constitutional province of Callao is considered part of the city of Lima and forms the Lima Metropolitan Area. Metropolitan Lima (ML) has more than 9.5 million residents (32.6% of the national population) and an unplanned population growth of 1.2% per year according to the 2017 census [1]. A total of 36% of the ML population lives on unstable slopes [2], while infrastructure, economic activities, the environment, and the population's health are exposed to natural hazards.

Extreme Meteorological Events (EMEs) could be more frequent and intense in the context of climate change [3]. The Intergovernmental Panel on Climate Change (IPCC) highlighted the importance of characterizing the trends of extreme weather events to understand the climate and assess the effects of global warming and thus develop appropriate strategies to minimize impacts [4,5]. The research on climatic extremes has developed enormously in the last few decades.

Studies of extreme events around the globe show significant warming trends in all temperature-related indices. For example, there was a significant increase in warm nights and warm days during 1901–2010. On the other hand, most precipitation indices show a

tendency toward wetter conditions, but not all show statistically significant changes [6,7]. For South America, there is evidence of warming and wetting since the mid-20th century onwards (e.g., minimum temperature indices show the largest rates of warming, while maximum temperature indices show a lower rate of warming). The total amount of annual precipitation increased, particularly over Amazonia and southeast of South America [8]. Various results were found in the climate extreme trends on a national scale, as a consequence of the complex topography and climate of Peru. Changes in precipitation extremes are spatially more complex and less significant. The total annual precipitation shows stressed increases (positive trend) over the northern coast, while the northern jungle shows some decreases (negative trend) from the 1960s until the end of the last century. On the other hand, the indices of temperature climate extremes show a decrease in the cold days and an increase in the warm days, except for the northern jungle [9]. Significant negative trends in extreme precipitation indices were found in the northern and southern parts of the Mantaro basin during 1965–2006; while the extreme temperature indices are quite variable, there is a negative trend in the number of frost days and positive trends in warm days and warm nights in the central area of the basin [10]. There are no significant trends in extreme precipitation indices in Peruvian Altiplano during the period 1971–2013 [11].

Likewise, the possible future changes of the extremes until 2050 were analyzed using the information of regional climate scenarios from the National Service of Meteorology and Hydrology of Peru (SENAMHI), and the results indicate increases in the frequency and intensity of rainfall over the central and southern coasts, while, for temperature, an increase of more than 1.5 °C on coast was predicted, increases in extreme temperature indices were also identified, such as warm nights and warm days [12]. In this context, there will be a strong spatial and temporal variability of the occurrence of EMEs in Peru, which would cause different impacts in various localities. Therefore, local research is important for the authorities to develop adaptation strategies for possible disasters. Specific studies have been carried out in certain regions of Peru. However, there is still a lack of studies on the behavior of climate extreme indices both in urban and overpopulated areas, such as the case of Lima.

The most extreme event of precipitation in ML happened on 15 January 1970, with exceptional precipitation of 16 mm in one day. Some impacts of this extreme event were the following. This heavy rainfall flooded the streets of the city; there were fires caused by short-circuits in public and domestic lighting; power failures occurred in Miraflores, Magdalena, and La Victoria; telephone communications collapsed; the Jorge Chávez international airport facilities were seriously damaged; nearly two thousand homes were destroyed; the highway that connects Lima to Chosica was blocked by landslides during the night; the Rímac, Chilca, and Chillón rivers increased their flow that caused overflow; in the Armendáriz ravine, the water flowed like waterfalls; and nine injuries and one death (Cabat Ballón Torres, Mechanic) in Collique were reported [13–15]. There are multiple factors that triggered this disaster, mainly the geomorphological and climatic factors of the Lima region. ML's vulnerability will increase due to the occurrence of hydrometeorological phenomena caused by the climate change.

In coastal areas of the Peruvian Pacific (south of 7° S), those where dry conditions prevail and there is no rainfall can be affected by extreme daily rainfall of more than 10–15 mm during strong El Niño events, this can constitute a threat to the area [16,17]. El Niño Southern Oscillation (ENSO) is projected to remain the dominant mode of interannual variability with global influence, and, due to increased moisture availability, ENSO-induced rainfall variability will intensify on regional scales [18].

The objective of this study was to carry out a local analysis of climate variability and extreme climate indices based on temperature and precipitation in ML. In addition, the most extreme precipitation event that occurred in Lima was studied. This research will provide basic information that can be used as a useful resource to assess ML vulnerability and thus manage and adopt measures to establish appropriate public politics to reduce the impacts of EMEs on the population.

This article is organized as follows. Section 2 provides a brief description of the study area, data set, and the methodology used in this research. Section 3 presents the main results and discussions. It includes Section 3.1, which presents a characterization of the ML climate, based on a monthly and seasonal analysis of temperature and precipitation. Section 3.2 provides an assessment of the interannual variability of precipitation and temperature and its relationship to regional patterns. Section 3.3 analyzes the trends of the variables studied. Section 3.4 describes the extreme climate indices of temperature and precipitation. Section 3.5 provides a brief analysis of the most extreme precipitation event in Lima. Finally, Section 4 presents the conclusions of the article.

2. Materials and Methods

2.1. Study Area

Figure 1a–c show the study area (ML) that comprises the urban centers of the Lima and Callao provinces. ML is located on the central-western coast of the Peruvian territory, in the middle of the western side of the South American continent, between $11^{\circ}45'–12^{\circ}24'$ South Latitude and $76^{\circ}40'–77^{\circ}10'$ West Longitude. ML has an area of 2812 km^2 , of which 798.6 km^2 are urbanized, 179.9 km^2 are farmland, and 1833.5 km^2 are mountainous land with little chance of being urbanized [19]. ML has around one third of the country's total population [1,20]. The topography is relatively flat, with an average altitude of 154 m above sea level. The important changes in its relief occur in the east, in which areas of foothills and small mountains appear. This city lies at the junction of three coastal valleys formed by the rivers descending from the Andean highlands [21].

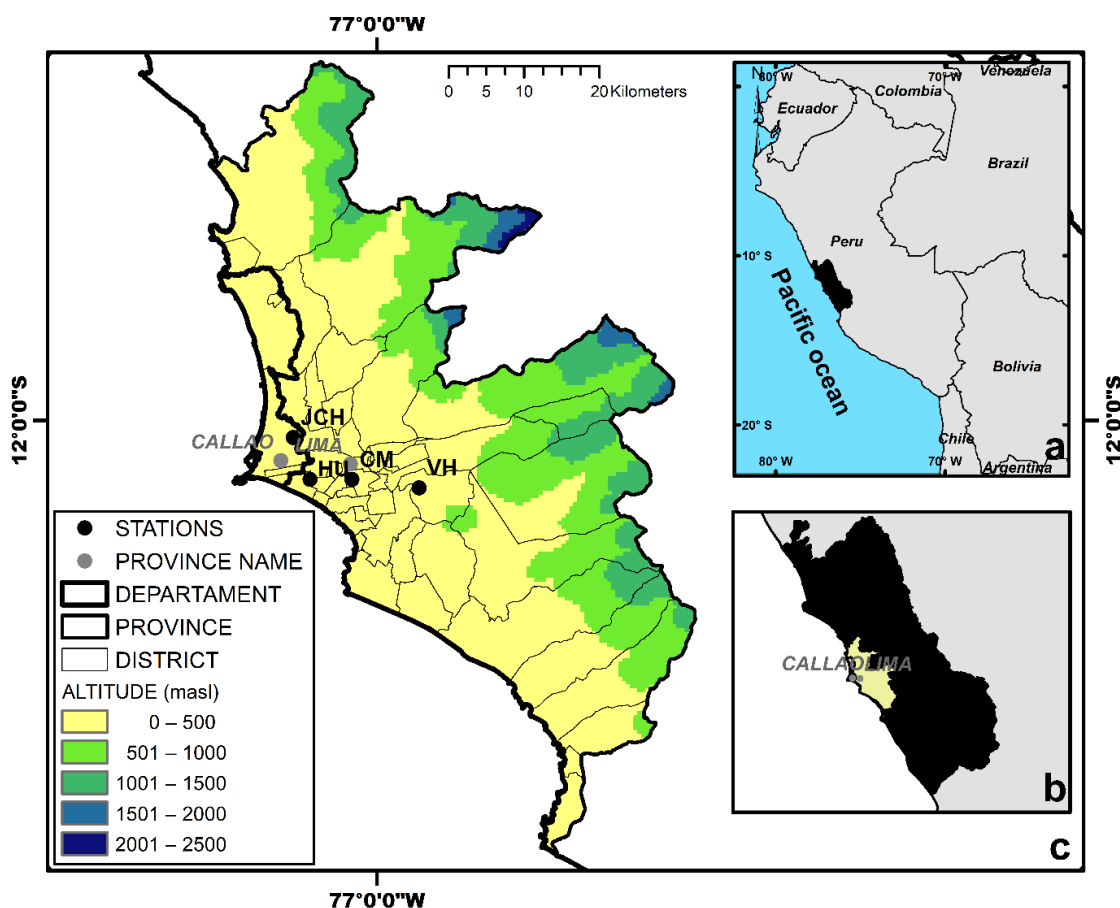


Figure 1. Location of Metropolitan Lima (ML): (a) South America, (b) Department of Lima, (c) Province of Lima and Callao. The black dots represent the location of the stations used in this study, and the gray dots represent the capitals of Lima and Callao.

The Rimac river crosses the urban area to lead north of the Callao port. The population depends on rivers that flow from the Andes for water for consumption [20]. ML limits to the east with the foothills of the central Andes Mountain Range and to the west with the Pacific Ocean.

ML has a desert ecosystem with little rain. The climatic conditions are influenced by the persistent atmospheric stability, which is caused by the interaction of the South Pacific anticyclone, the cooling power of the Von Humboldt Ocean current, and the presence of the Andes Mountain Range; therefore, ML does not present tropical climatic characteristics [22–24]. The predominant climate of Lima is arid and temperate, with moisture deficiency in all seasons of the year according to the latest national climate classification [24]. A detailed description of the meteorological variables of temperature and precipitation will be provided in Section 3.1.

2.2. Data

We used daily datasets of observed precipitation and temperature for the period 1965–2013. Climatological stations with more than 30 years of data were considered for this study. Station names and the lengths of each record are listed in Table 1. The data of the Hipólito Unanue (HU, West Lima) were obtained from the Physics Department of the Pontifical Catholic University of Peru (PUCP), the data of Jorge Chávez (JCH, Callao) were obtained from the Peruvian Airports and Commercial Aviation Corporation (CORPAC), and the data of Von Humboldt (VH, East Lima) were obtained from the National Agrarian University of La Molina (UNALM). Additionally, the monthly data of the mean temperature from Campo de Marte station (CM, center Lima) were used.

Table 1. List of climatological stations used in this study. Maximum temperature (TX), Minimum temperature (TN), average temperature (TP), and precipitation (PP).

Station Name	Latitude (S)	Longitude (W)	Altitude (masl)	Variables	Information Period
Hipólito Unánue (HU)	12°04′	77°05′	70	TX, TN, PP	1 June 1968 to 31 December 2013
Jorge Chavez (JCH)	12°01′	77°06′	34	TX, TN, PP	1 January 1963 to 31 December 2013
Von Humboldt (VH)	12°05′	76°57′	244	TX, TN, PP	1 January 1965 to 31 December 2007
Campo de Marte (CM)	12°04′	77°02′	123	TP	June 1931 to December 1981

We used monthly SST indices as oceanic indicators for different sectors of the tropical Pacific Ocean. Dataset was obtained from the Climate Prediction Center of the National Oceanic and Atmospheric Administration (CPC/NOAA); data are freely available at <https://www.cpc.ncep.noaa.gov/data/indices/> (accessed on 28 May 2022). The Niño 1+2 SST index is an indicator of far eastern tropical Pacific El Niño conditions, off the coasts of Peru (0–10° S, 90°–80° W), the Niño 3 SST index is an indicator of the eastern tropical Pacific (5° N–5° S, 150°–90° W), the Niño 3.4 SST index is an indicator of central tropical Pacific El Niño conditions (5° N–5° S, 170°–120° W), and the Niño 4 SST index is an indicator of western tropical Pacific El Niño conditions (5° N–5° S, 160° E–150° W) [25–27].

We used reanalysis data from the National Centers for Environmental Prediction/National Center for Atmospheric Research (NCEP-NCAR) [28] of SST and wind at 200 hPa, 500 hPa, 850 hPa, and 925 hPa levels. This database provides a numerical description of the current climate, and these data are derived by a combination of models with observed data. Moreover, we used water vapor flux ($\text{kg m}^{-1} \text{s}^{-1}$) between 1000 hPa and 300 hPa obtained from NCAR reanalysis data with a 2.5-degree spatial resolution.

2.3. Methods

Daily data of temperature and precipitation were subjected to quality control before being used in the extreme indices analysis. RCLimDex QC software was used for this

purpose [29]. The following procedure was performed: (1) it has been controlled so that there are no duplicate or out-of-sequence dates in the daily observations; (2) all missing values were replaced (currently coded as -99.9), NA is not available; and (3) all unreasonable values were replaced, those values include: (a) daily precipitation amounts less than zero, (b) daily maximum temperature less than daily minimum temperature, (c) daily temperature values greater than 70 degree Celsius or less than -70 degree Celsius, (d) all values corresponding to an impossible date (i.e., 32 April 2012, 12 June 20AA), and (e) any non-numeric values. In addition, (4) QC also identifies outliers in the daily maximum and minimum temperatures. The outliers are daily values outside a region defined by the user. Currently, this region is defined as the *mean* plus or minus n times standard deviation of the value for the day:

$$\text{Outliers} = [\text{mean} \pm n * \text{std}], \quad (1)$$

where *std* represents the standard deviation for the day, n is an input from the user, and the *mean* is computed from the climatology of the day. The identification of outliers in temperature data requires input from the user. We used the default value for n , which is 3. Then, the data was checked to determine if any value marked as an outlier is really an outlier.

The temperature and precipitation climatologies were calculated based on the period from 1981 to 2010. The average temperature (TP) was estimated between the average of the minimum temperature (TN) and the maximum temperature (TX). To reconstruct the TP record of CM station, a linear regression analysis was performed between the TP series of the HU, VH, and JCH stations. Linear regression analysis is a parametric model and one of the most common methods used to detect a pattern in data series. Moreover, the linear correlation coefficient (r) was calculated to determine the usefulness of the statistical inference; a value greater than 0.97 and a p -value < 0.05 were obtained in all cases, which indicates a good match. The linear regression model is generally described by the following equation [30]:

$$Y = m * X + C, \quad (2)$$

where Y and X are the dependent variable and the independent variable, respectively, m is the line slope, and C is the intercept constant coefficient. The coefficients (m and C) of the model are determined using the Least-Squares method, which is the most commonly used method. The slope sign defines the trend variable direction; it increases if the sign is positive and decreases if the sign is negative.

Extremely rainy, very rainy, and rainy years were identified using the 99th, 95th, and 90th percentiles, respectively, as was conducted by Ref. [31]. Furthermore, those years with rainfall greater than the 90th percentile (less than the 10th percentile) were considered extreme rainy (dry) years. Likewise, those years with temperatures greater than the 90th percentile (less than the 10th percentile) were considered extreme warm (cold) years.

Annual trends were estimated for the temperature, precipitation, and extreme indices time series. A combined Mann–Kendall (MK) test [32,33] and Sen' slope [34] approach were applied to these time series. This MK test does not require that the data be normally distributed or linear, that is, this nonparametric test can be used in a time series without assuming any particular distribution. The statistic of the Mann–Kendall test (S) [32,33] is defined as:

$$S = \sum_{i=1}^{n-1} \sum_{j=i+1}^n \text{sgn}(x_j - x_i), \quad (3)$$

where x_i and x_j are the sequential data, n is the total amount of data in the time series and

$$\text{sgn}(\Delta x) = \begin{cases} 1, & \Delta x > 0 \\ 0, & \Delta x = 0 \\ -1, & \Delta x < 0 \end{cases} \quad (4)$$

A positive (negative) value of S indicates an ever-increasing (downward) trend. Nevertheless, the statistical analysis of the validity of the phenomenon needs to be carried out. The variance (S) is calculated with the following equation:

$$Var(S) = \frac{n(n-1)(2n+5) - \sum_{i=1}^m t_i(t_i-1)(2t_i+5)}{18}, \quad (5)$$

where n is the number of data points, m is the number of tied groups, and t_i denotes the number of ties of extent i . A tied group is a set of sample data having the same value. In cases where the sample size $n > 10$, the standard normal test statistic Z is:

$$Z = \begin{cases} \frac{S-1}{\sqrt{Var(S)}}, & S > 0 \\ 0, & S = 0 \\ \frac{S+1}{\sqrt{Var(S)}}, & S < 0 \end{cases} \quad (6)$$

At significance level α , the null hypothesis of no trend is rejected if the absolute value of Z is greater than the theoretical value $Z_{1-\alpha/2}$, which is obtained from the standard normal distribution table. In this study, significance levels $\alpha = 0.05$ and $\alpha = 0.10$ were used. Further information related to the Mann–Kendall test can be found in Ref. [35].

In addition, the Sen slope estimator [34] was used, which is also a nonparametric method, and it is a method for robustly fitting a line to sample points in the plane (simple linear regression) by choosing the median of the slopes of all lines through pairs of points. The Sen slope has the advantage over the ordinary linear regression slope, because it is not affected by individual data errors and outliers [36]. The magnitude of the slope of the trend was estimated as:

$$Q_o = \frac{x_i - x_j}{j - i} \text{ for } o = 1, \dots, N, \quad (7)$$

where x_i and x_j are data at times i and j ($j > i$), respectively. If there are n values in the time series, then $N = n(n-1)/2$ slope estimates are possible. Then, the N values of Q_o are ranked from smallest to largest and the median of Sen's slope estimator is:

$$Q_{med} = \begin{cases} Q_{\lfloor \frac{N+1}{2} \rfloor}, & \text{if } N \text{ is odd} \\ \frac{Q_{\frac{N}{2}} + Q_{\lfloor \frac{N+2}{2} \rfloor}}{2}, & \text{if } N \text{ is even} \end{cases} \quad (8)$$

The Q_{med} sign reflects the data trend, while its value indicates the steepness of the trend. A positive Sen's slope reveals an upward trend, while a negative Sen's slope suggests a downward trend.

The Pearson correlation coefficient (r) was calculated to measure the association degree between the different climate indices, which has the characteristic of being dimensionless and varies in a range of -1 and $+1$; this statistical parameter is described by Refs. [37,38].

To describe the large-scale circulation associated with extreme hot, cold, rainy, and dry years in ML, SST and wind composite anomalies at 200 hPa, 500 hPa, and 850 hPa levels were generated. Likewise, wind composite anomalies were calculated for days before and after the most extreme precipitation event in ML at 200 hPa, 500 hPa, 850 and 925 hPa levels. The 1981 to 2010 climatology was used to calculate the anomalies. Moreover, composites of water vapor flux for the date of extreme precipitation event between 1000 hPa and 300 hPa for 12, 18, and 00 UTC were calculated.

To assess the intensity and frequency of extreme precipitation and temperature events, this study employs 21 indices proposed by the team of experts on Climate Change Detection and Indices (ETCCDI) [39–42]. Daily precipitation and temperature data were used to identify extreme climate indices. The meanings of the indices, acronyms, and methods used in their calculations are summarized in Table 2. The methodology provides a standard measurement set of extreme climate indices and includes careful quality control of the data. Further information about the definitions and mathematical formulas of the extreme climate

indices can be found in Refs. [29,40]. We used the HU, VH, and JCH stations to describe the extreme temperature indices, while the HU station was considered in the analysis of extreme precipitation indices, because it is the largest and most complete series at the daily level for this variable, thus reducing the effect of the lost data values on the calculation of the indices. Taking into account the behavior of rainfall in ML, the threshold >0.1 mm was applied to identify a day with precipitation. This is consistent with the study carried out by SENAMHI on precipitation thresholds, in which days with rain are defined as precipitation accumulated in 24 h greater than 0.1 mm ($PP > 0.1$ mm) for arid zones such as Lima [31]. In this way, a common criterion would be used to define a rainy day for Lima and thus carry out an adequate characterization of extreme rainfall.

Table 2. Extreme temperature and precipitation indices selected for this investigation.

Indicator Name (ID)	Indicator Definitions	Units
Warm days (TX90p)	Annual percentage of days when TX $>$ 90th percentile in relation to the climatology from 1981–2010	%
Warm nights (TN90p)	Annual percentage of days when TN $>$ 90th percentile in relation to the climatology from 1981–2010	%
Cold days (TX10p)	Annual percentage of days when TX $<$ 10th percentile in relation to the climatology from 1981–2010	%
Cold nights (TN10p)	Annual percentage of days when TN $<$ 10th percentile in relation to the climatology from 1981–2010	%
Max TX (TXx)	Monthly maximum value of daily TX	$^{\circ}$ C
Max TN (TNx)	Monthly maximum value of daily TN	$^{\circ}$ C
Min TX (TXn)	Monthly minimum value of daily TX	$^{\circ}$ C
Min TN (TNn)	Monthly minimum value of daily TN	$^{\circ}$ C
Warm spell duration indicator (WSDI)	Annual count of days with at least 6 consecutive days when TX $>$ 90th percentile	Days
Cold spell duration indicator (CSDI)	Annual count of days with at least 6 consecutive days when TN $<$ 10th percentile	Days
Annual total wet-days precipitation (PRCPTOT)	Annual total precipitation in wet days (precipitation $>$ 0.1 mm)	mm
Extremely wet days (R99p)	Annual total precipitation when precipitation $>$ 99th percentile	mm
Very wet days (R95p)	Annual total precipitation when precipitation $>$ 95th percentile	mm
Simple daily intensity index (SDII)	Annual total precipitation divided by the number of wet days (defined as precipitation $>$ 0.1 mm) in the year	mm/day
Number of days above 1 mm (R1mm)	Annual count of days when precipitation $>$ 1 mm, 1 is user defined threshold	Days
Number of days above 2 mm (R2mm)	Annual count of days when precipitation $>$ 2 mm, 2 is user defined threshold	Days
Max 1-day precipitation amount (Rx1day)	Maximum precipitation in 1 day	mm
Max 5-day precipitation amount (Rx5day)	Maximum precipitation in 5 consecutive days	mm
Max 10-day precipitation amount (Rx10day)	Maximum precipitation in 10 consecutive days	mm
Consecutive wet days (CWD)	Maximum number of consecutive days with precipitation $>$ 0.1mm	Days
Consecutive dry days (CDD)	Maximum number of consecutive days with precipitation \leq 0.1 mm	Days

3. Results and Discussion

3.1. Precipitation and Temperature Climatology in ML and Its Links with the SST

The annual TP of ML is 19.9 °C with a standard deviation of ±1.3 °C. Figure 2a–f illustrates a well-defined seasonality between summer and winter in ML. Figure 2a,d shows that the highest TP is reached in summer, in February (23.9 °C ± 1.1 °C), and the coldest month in the winter is August (16.8 °C ± 1.3 °C). The temperature in Lima is much lower than those expected for a tropical coastal desert (12° South Latitude), due to the climate conditions mentioned in item 2.1, which cause high subsidence and abundant low-stratiform cloudiness that prevent the effective action of solar radiation, especially in winter [22]. All these factors maintain the temperature without great ranges.

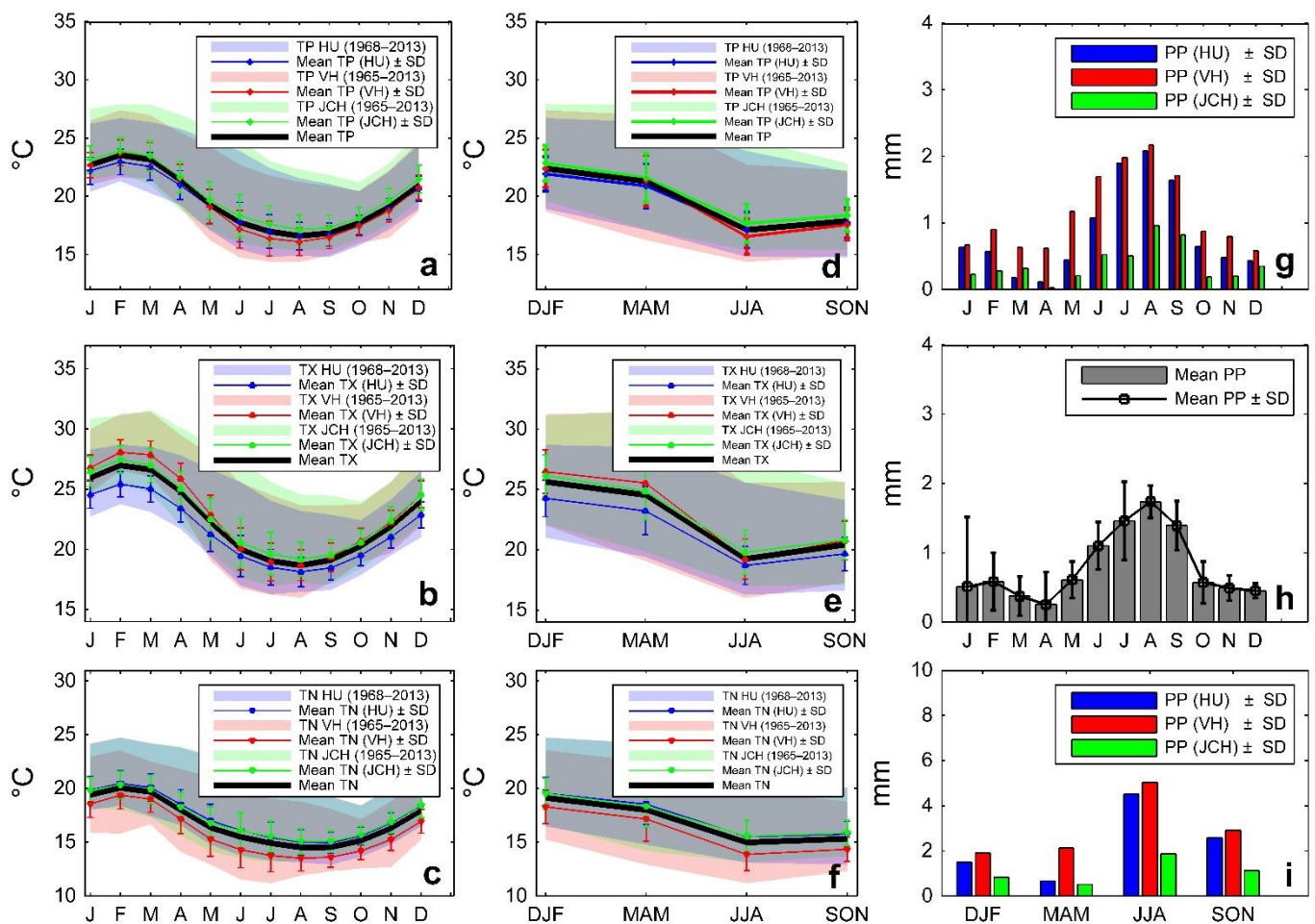


Figure 2. Monthly (a–c) and seasonal (d–f) climatology of maximum temperature (TX), minimum temperature (TN), and average temperature (TP). Monthly (g,h) and seasonal (i) precipitation (PP) in Metropolitan Lima. Climatology base period 1981–2010. Hipolito Unanue (HU), Von Humboldt (VH), and Jorge Chavez (JCH) weather stations.

Regarding the extreme values of temperature (TX and TN), Figure 2b,c shows that the maximum average of TX (TN) is 27.3 °C ± 1.1 °C (20.4 °C ± 1.2 °C) registered in February, while the minimum average of TX (TN) is 18.9 °C ± 1.3 °C (14.7 °C ± 1.2 °C) recorded in August. Figure 2b shows that the thermal range of TX between stations near the sea (HU, JCH) is 2.1 °C (1.1 °C) in summer (winter). Moreover, the thermal range of TX increases with respect to the distance from the sea in summer (Figure 2e). The same does not happen with TN, which has very similar values between stations near the sea (Figure 2f).

On the other hand, rainfall is definitely scarce in ML, usually occurring in drizzle form during a large part of the year due to the condition of high subsidence. The average PP in

Lima is 9.1 mm/year, with a standard deviation of ± 1.0 mm/year, which is consistent with the findings reported in other studies [24]. Figure 2g–i shows that the greatest variability of PP is centered in winter and early spring. Figure 2i shows that the highest values of PP are reached in winter (≈ 5.5 mm). Moreover, drizzles predominate in the winter season due to local-scale processes (strong marine cooling, strong coastal winds at lower levels, and a strong atmospheric inversion) [22,23]. In summer, some occasional rainfall has a regional-scale influence, associated with the presence of the Bolivian High (BH), the convection development, and rains developed in the Andean areas, that can cause the transfer rains toward the coast due to the passage of humid air masses from the Atlantic Ocean through the mountain range at high and mid levels [23].

In general, the temperature variability in Lima is linked to SST variations in the tropical Pacific Ocean. Figure 3a displays a strong association between SST in the Eastern Tropical Pacific (Ecuador, Peru, and northern Chile coasts) and TX in Lima. Likewise, Figure 3b shows that the thermal variations in the Eastern Tropical Pacific also have a great contribution to the TN variability in Lima. The relationship between SST in the Niño 1+2 region and temperature (TX, TN) in ML is strong and positive ($+0.90 \geq r \geq +0.85$; $p < 0.05$). This indicates that the warming of SST in the Niño 1+2 region would cause an increase in temperatures in Lima. The association between SST in the eastern sector (Niño 3 region) and temperature in ML is moderate and significant ($+0.61 \geq r \geq +0.50$; $p < 0.05$). The relationship between SST in the western Pacific (Niño 4 region) and temperature in Lima is weak and negative ($-0.24 \leq r \leq -0.07$; $p < 0.23$). The association between SST in the central sector of the tropical Pacific (Niño 3.4 region) and temperature in ML is weak but significant ($+0.11 \geq r \geq +0.30$; $p < 0.05$). The marine thermal variations of the Atlantic Ocean also affect the temperature of Lima, although the associations are quite variable in sign and distribution.

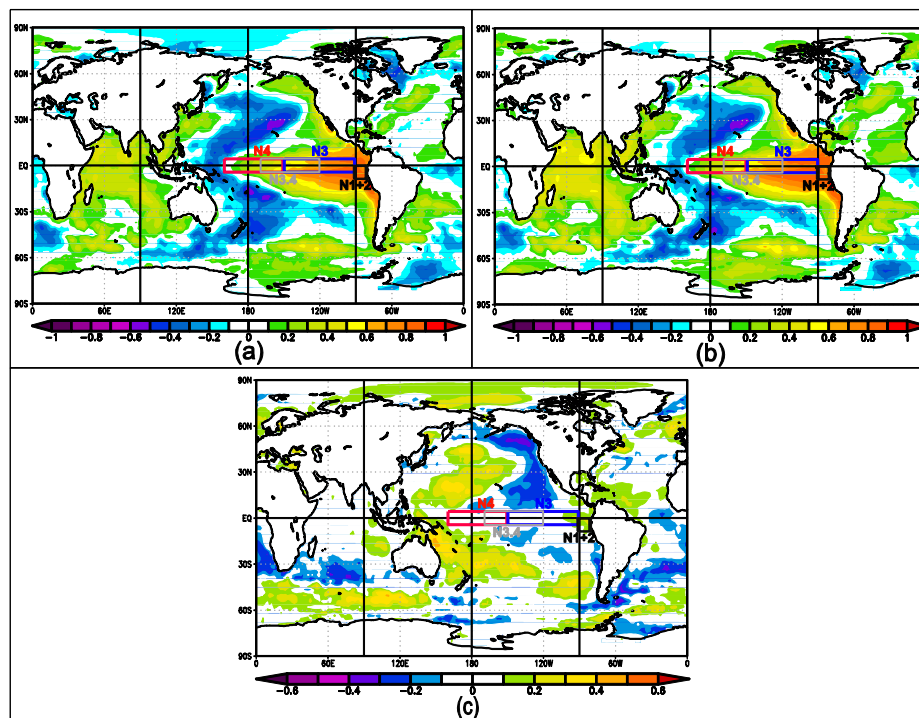


Figure 3. Spatial field of annual correlations between Sea Surface Temperature (SST) and (a) maximum temperature (TX), (b) minimum temperature (TN), and (c) precipitation (PP) in Lima. Niño SST indices corresponding to the regions Niño 1+2 (N1+2), Niño 3 (N3), Niño 3.4 (N3.4), and Niño 4 (N4). Analysis carried out for Hipolito Unanue (HU) station during the period 1968–2013. NCEP/NCAR Reanalysis. Source: NOAA/ESRL Physical Sciences Laboratory.

Figure 3c displays the weak association between SST in the tropical Pacific Ocean and PP in Lima. It should be noted that there is no great contribution of adjacent oceans' SSTs on the rainfall variability in ML. Only in some months of the year, there are correlations around 0.4 with areas of the central and eastern Pacific, which could be associated with processes linked to El Niño events. Likewise, other researchers affirm that coastal southern Peru can be affected by heavy rains during strong El Niño events [16,17].

3.2. Interannual Variability of Temperature and Precipitation in Lima and Its Association with Regional Patterns

The extreme warm years in ML (1972, 1983, 1987, 1992, 1997, 1998) are associated with the warm phase of ENSO. The SST in the eastern and central Pacific presented positive anomalies (greater than +0.5) during extreme warm years; the maximum values (+3.0 °C) were found in April, May, and June. Figure 4a shows the positive anomaly of SST (+1.8 °C) on the north and central coast of Peru in the warmest month of the year (February). Figure 4c displays that westerly wind anomalies toward the Peruvian coast prevailed at high levels of the atmosphere during the extreme warm years. This is due to the Walker circulation modification attributed to the occurrence of El Niño, with the total weakening of the trade winds from the south and southeast, even during the winter season. Westerly winds toward the Peruvian coast weaken at mid and low levels of the atmosphere (not shown) during the extreme warm years, favoring the entry of a moisture flux from the Amazon toward the Peruvian highlands.

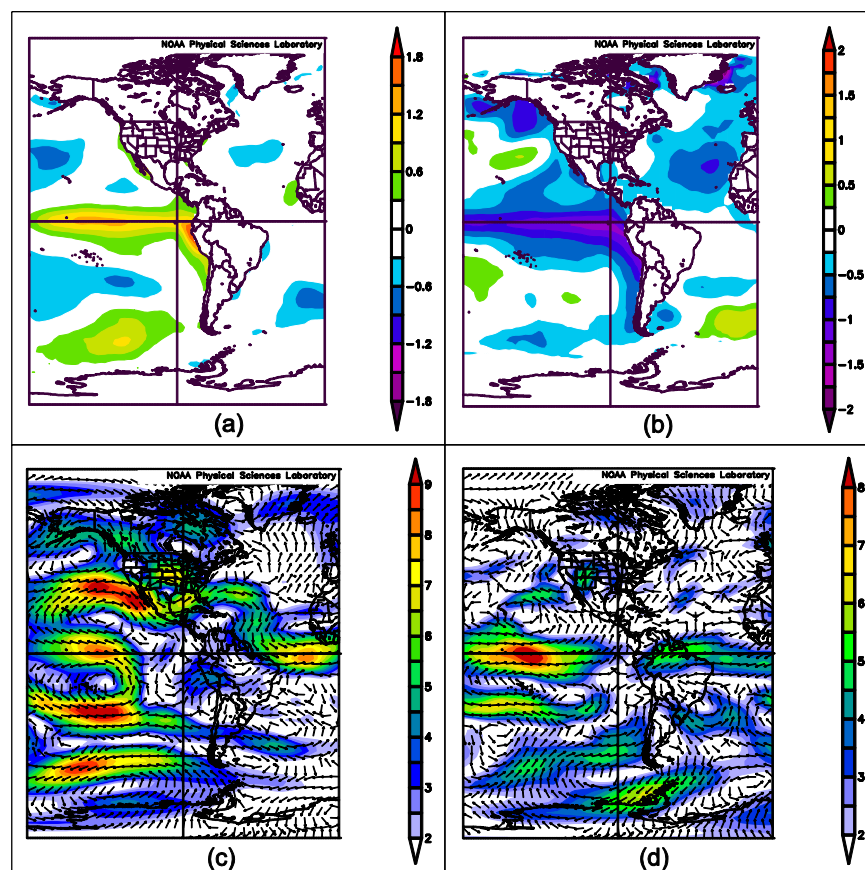


Figure 4. Composite anomalies of Sea Surface Temperature (SST) for extreme (a) warm years in February and (b) cold years in August. Composite anomalies of winds at 200 hPa associated with extreme (c) warm years in February and (d) cold years in August in Metropolitan Lima. Anomalies in °C for the SST and m/s for winds, their ranges are shown in the vertical color bars to the right of each figure. Data are from the NCEP/NCAR Reanalysis. Climatology 1981–2010. Source: NOAA Physical Sciences Laboratory.

The extreme cold years in ML (1970, 1971, 1973, 1974, 1975, 1996, 2007) present opposite characteristics to the warm periods. The extreme cold years are associated with the cold phase of ENSO. The SSTs in the eastern and central Pacific present negative anomalies during extreme cold years (from $-1.7\text{ }^{\circ}\text{C}$ to $-0.5\text{ }^{\circ}\text{C}$). Figure 4b shows a negative anomaly of SST ($-1.7\text{ }^{\circ}\text{C}$) on the north and central coast of Peru in the coldest month of the year (August). Figure 4d shows that easterly winds toward the Peruvian coast prevail at the high level of the atmosphere during the extreme cold years. Easterly winds toward the Peruvian coast weaken at mid and low levels of the atmosphere (not shown) during the extreme cold years.

Of the extreme rainy years in ML (1970, 1971, 1983, 2008, and 2009), the most notorious influence of El Niño on rainfall was during 1983, 2008, and 2009 years. Figure 5c shows positive biases of PP (11.8, 10.4, and 14.1 mm) during the 1983, 2008, and 2009 El Niño events, respectively. Rainfall in 1971 was influenced by the strong magnitude La Niña event of that year. The rainfall in 1970 (34.1 mm) was 40% higher than the rains during the extraordinary El Niño event of 1982/83; the most extreme precipitation event in Lima occurred during this year, which is not associated with La Niña event. There is no robust influence of Tropical Pacific SST on the extreme precipitation years. The atmospheric circulation in extreme rainy years is not well defined at high levels. However, the predominant circulation is from the east, northeast, and north towards the Peruvian coast at medium and low levels during a large part of the year.

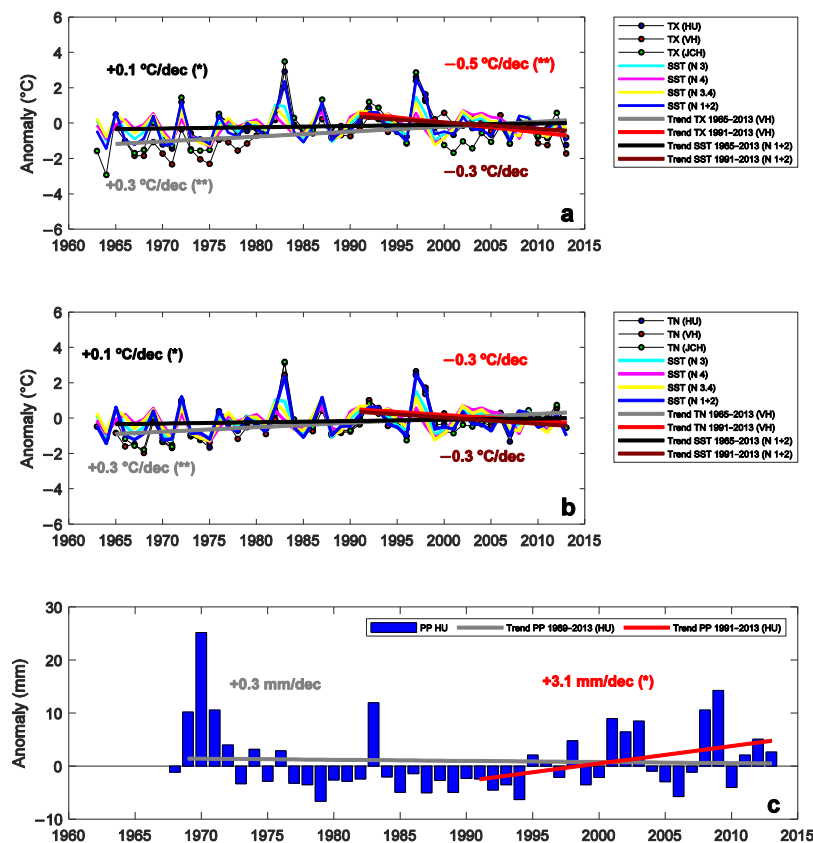


Figure 5. Linear trends for annual series of (a) maximum temperature (TX) and Niño 1+2 SST index, (b) minimum temperature (TN) and Niño 1+2 SST index and (c) precipitation (PP). Hipólito Unanue (HU), Von Humboldt (VH), and Jorge Chavez (JCH) stations. Niño SST indices corresponding to the regions Niño 1+2 (N1+2), Niño 3 (N3), Niño 3.4 (N3.4), and Niño 4 (N4). ** Statistically significant trends at the 95% confidence level ($p < 0.05$). * Statistically significant trends at the 90% confidence level ($p < 0.10$). Period 1965–2013.

The extreme dry years in ML (1979, 1985, 1987, 1989, 1994, 2006) are also not related to SST alterations in the adjacent oceans. Defined atmospheric circulations were not found, the circulations have been variable in the different levels of the atmosphere.

3.3. Temperature and Precipitation Trends

The temperature (TX and TN) in ML shows a slight trend towards warm conditions for the period 1965–2013. Particularly, TX and TN in East Lima (VH) show a significant increase of $+0.3$ °C/decade for the period 1965–2013 (Figure 5a,b). The temperature in ML tends to decrease in shorter periods (1976–2013, 1979–2016, and 1991–2013). TX decreases significantly in East Lima (-0.5 °C/decade) from 1991 to 2013 (Figure 5a). This tendency is also observed in TN (-0.3 °C/decade) for the same region but is non-significant (Figure 5b). It is interesting to note that, in the last two decades, TX and TN have decreased compared to the last five decades, which is consistent with similar trends found for South American coastal areas by other researchers [43–45]. Likewise, SST in the Niño 1+2 region has significantly increased ($+0.1$ °C/decades, $p > 0.1$) for the period 1965–2013. Then, there is a certain decreasing trend of SST in the Niño 1+2 region at a rate of -0.3 °C/decade during the period 1991–2013.

Figure 6 shows TP in central Lima (CM) trends for different periods from 1931 to 2013. Overall, there is a slight warming of $+0.1$ °C/decade (p -value < 0.05) during 1931–2013, this trend reverses after the mid-70s, some cooling trend is shown during 1976–2013 (-0.2 °C/decade, p -value < 0.1), and the cooling intensifies (-0.5 °C/decade, p -value < 0.05) in the last two decades (1991–2013). Likewise, other researchers found cooling trends ranging between -0.2 and -0.4 °C/decade for the SST on the central and southern coast of Peru (Callao, Pisco, San Juan, and Ilo) since the mid-70s [44]. Moreover, temperatures are decreasing (-0.2 °C/decade) along the subtropical west coast of South America (central and northern coast of Chile) since the late 1970s [45]. Therefore, there is a contrast between the cooling in the coastal stations and the increase in atmospheric temperature in the Andes ($+0.25$ °C/decade) and in general with the global mean temperatures of recent decades [43–45].

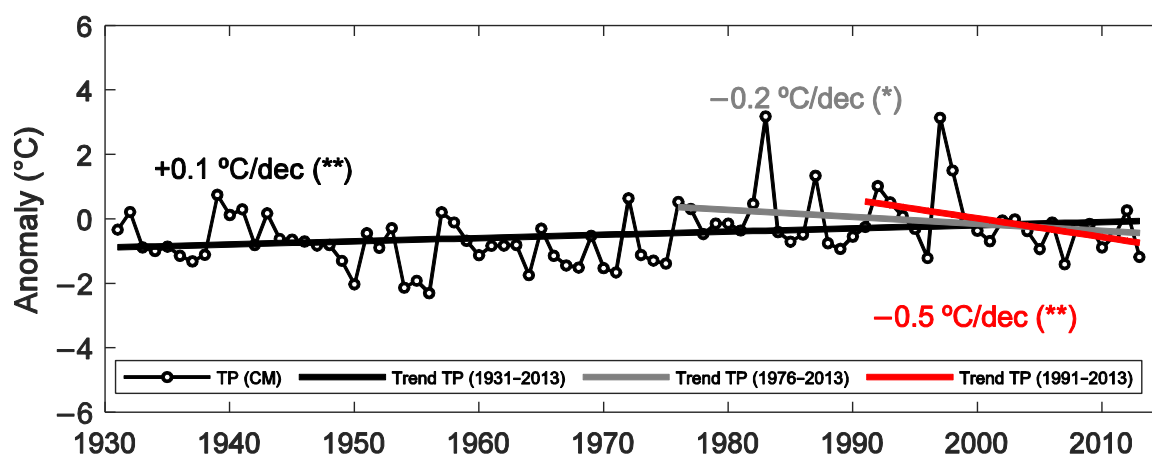


Figure 6. Linear trends of the reconstructed average temperature (TP) in central Lima (CM station) for the periods 1931–2013 (black line), 1976–2013 (gray line), and 1991–2013 (red line). ** Statistically significant trends at the 95% confidence level ($p < 0.05$). * Statistically significant trends at the 90% confidence level ($p < 0.10$).

Some causes associated with coastal cooling suggest possible factors on a regional scale, and others are more local, such as the intensification of the South Pacific Anticyclone during the last decades [45], the intensification of the winds along the coast, and the increased upwelling [43,44]. Moreover, other areas of the globe with strong coastal upwelling processes are presenting cooling between ranges of -0.2 and -0.7 °C/decade, such as

northwest and southwest Africa, associated with the cold currents of Canaria and Benguela, respectively [44].

Figure 5c shows PP in ML trends. There is no trend during the period 1969–2013. However, there is a certain increase in rainfall at a rate of +2 mm/decade from 1979 to 2013 and +3.1 mm/decade from 1991 to 2013.

3.4. Temperature and Precipitation Extremes in ML

3.4.1. Extreme Temperatures

Figure 7a shows the percentage of warm days (TX90p), and Figure 7c shows the percentage of warm nights (TN90p), both indices display no trends during 1965–2013. However, it should be noted that these percentages increased significantly during the extraordinary El Niño events of 1982–1983 and 1997–1998. ML registers less than 10% of TX90p and TN90p per year, these percentages increased until 74 and 79% of TX90p and TN90p, respectively, during the extraordinary El Niño event of 1982–1983.

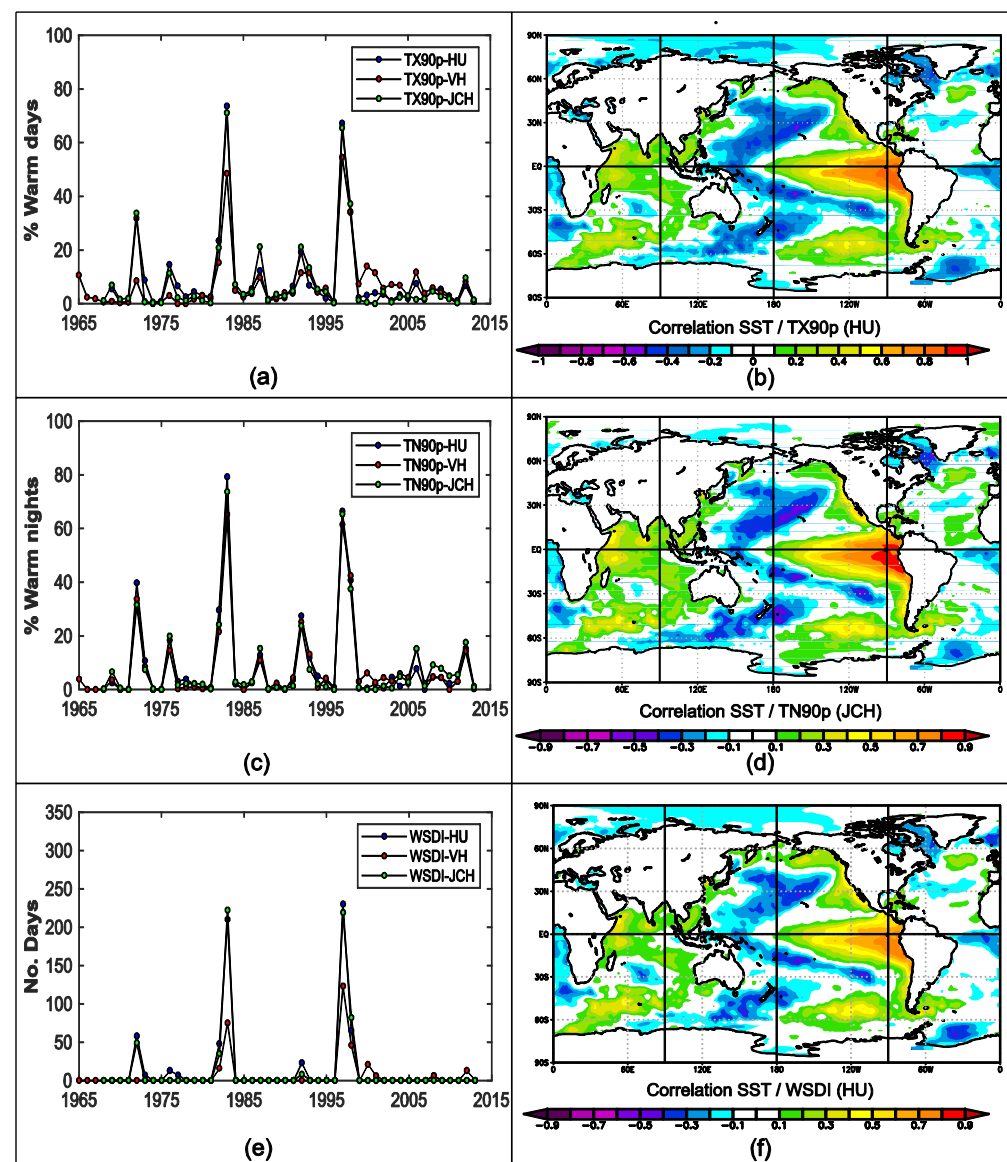


Figure 7. Variability and trends of extreme temperature indices: (a) TX90p, (c) TN90p, and (e) WSDI, these indices show no trend. Spatial field of annual correlations between Sea Surface Temperature (SST) and (b) TX90p, (d) TN90p, and (f) WSDI for the period 1965–2013. HU, VH, and JCH station. NCEP/NCAR Reanalysis. Source: NOAA/ESRL Physical Sciences Laboratory.

The influence of El Niño/La Niña events on the duration of heat waves (WSDI) and the duration of cold waves (CSDI) is also clear. Figure 7e shows that the maximum number of days (210 and 230) of WSDI in HU occurred during the extraordinary El Niño events of 1982–1983 and 1997–1998, respectively. However, no trend is found.

On the other hand, a slight warming trend is observed in the extreme values of TX and TN in Lima from 1965 to 1998. Figure 8c shows a slight increase in the maximum value of TX (TXx) and minimum value of TX (TXn) at the rate of $+0.6\text{ }^{\circ}\text{C}/\text{decade}$ and $+0.5\text{ }^{\circ}\text{C}/\text{decade}$, respectively, between 1965 and 1998. Figure 8d shows an increase of $+0.8\text{ }^{\circ}\text{C}/\text{decade}$ in the maximum value TN (TNx) from 1965 to 1998, while the minimum value of TN (TNn) shows a significant increase of $+0.7\text{ }^{\circ}\text{C}/\text{decade}$ over the last 49 years (1965–2013). However, the warming of the extreme values of TX and TN has not been constant; starting in 1999, there was a slight cooling trend, and TXx shows a significant decrease of $-1.0\text{ }^{\circ}\text{C}/\text{decade}$. In addition, the highest values of TXx and TNx were recorded during the extraordinary El Niño events of 1982–1983 and 1997–1998. For example, a value of $33.9\text{ }^{\circ}\text{C}$ in TXx was recorded on 13 March 1998 in VH, and a value of $25.8\text{ }^{\circ}\text{C}$ in TNx was recorded on 7 February 1983, in JCH. On the other hand, the lowest values of TXn and TNn were recorded during La Niña events of 1970 and 1967, respectively. For example, a value of $13.7\text{ }^{\circ}\text{C}$ in TXn was recorded on 13 August 1970 in JCH, and a value of $7.6\text{ }^{\circ}\text{C}$ in TNn was recorded on 2 August 1967 in VH.

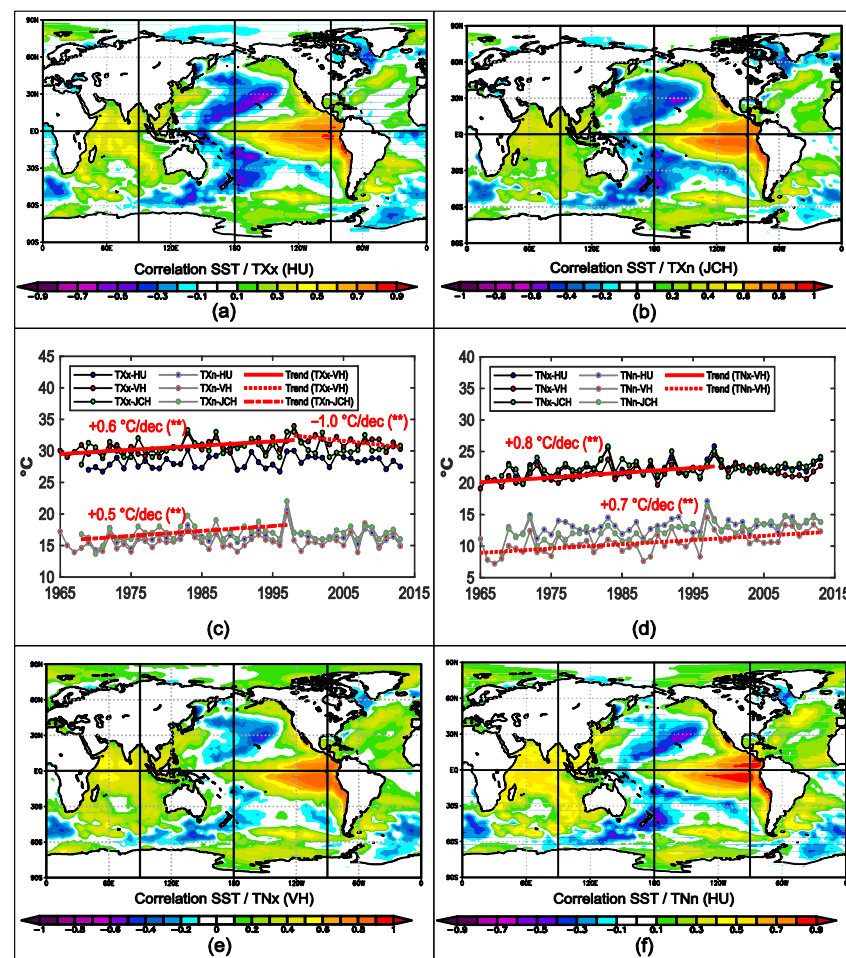


Figure 8. Spatial field of annual correlations between Sea Surface Temperature (SST) and (a) TXx, (b) TXn, (e) TNx, and (f) TNn for the period 1965–2013. Variability and trends of extreme temperature indices: (c) TXx and TXn and (d) TNx and TNn. HU, VH and JCH station. ** Statistically significant trends at the 95% confidence level ($p < 0.05$). NCEP/NCAR Reanalysis. Source: NOAA/ESRL Physical Sciences Laboratory.

Lima presents less than 14% of cold days (TX10p) and cold nights (TN10p) per year; these percentages increase during La Niña events. Figure 9a shows that TX10 increased to 53% in La Niña event of 1971, and Figure 9c shows that TN10 increased to 59% in the La Niña event of 1975. Furthermore, TX10p and TN10p have significantly decreased (-17.7% cold days/decade and -23.5% cold nights/decade, respectively) from 1965 to 1983 (Figure 9a,c); after this period, only TX10p shows a significant increase of $+2.2\%$ cold days/decade. Likewise, Figure 9e shows that the maximum number of TN days (149) of CSDI occurred during La Niña events of 1975.

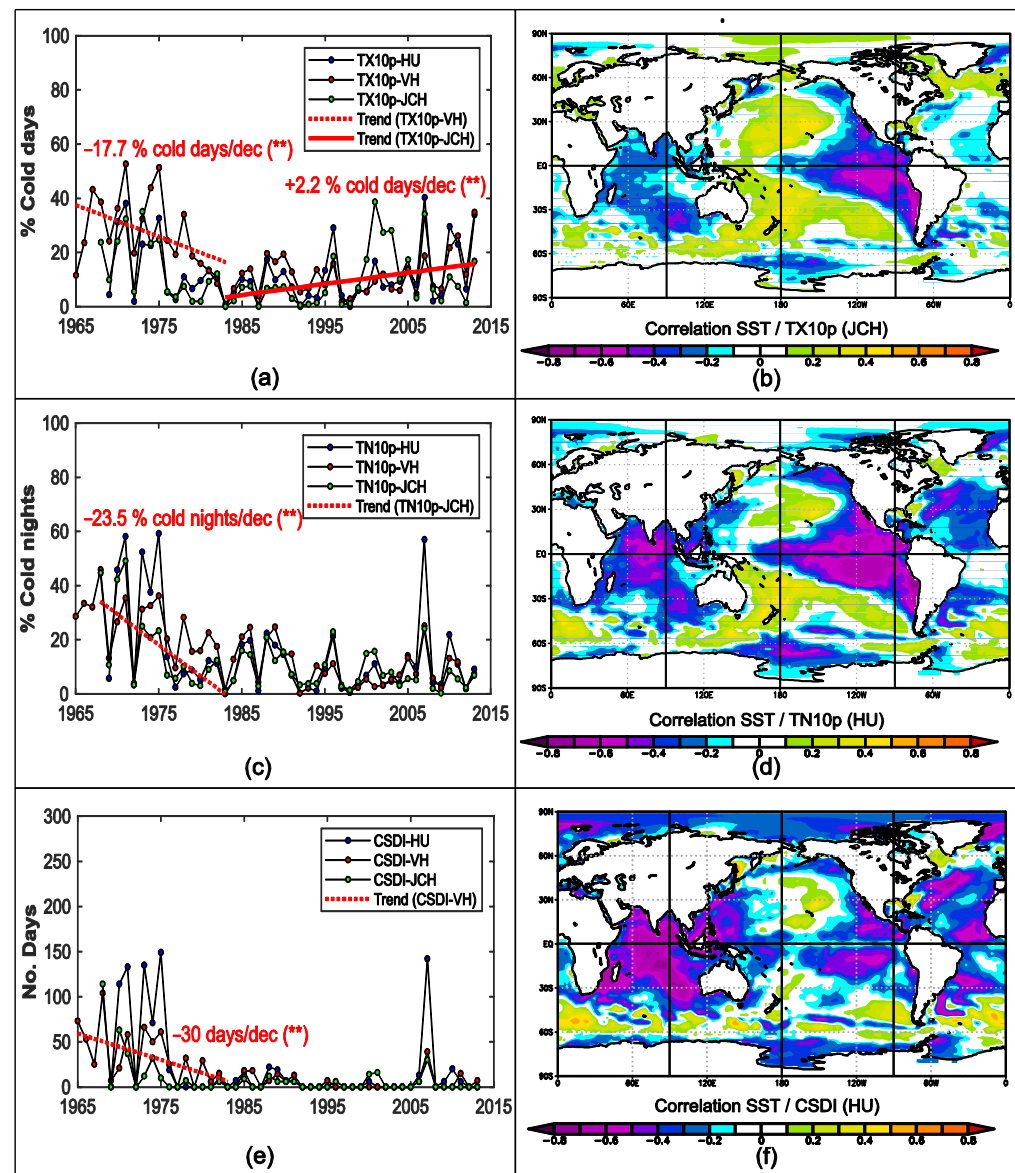


Figure 9. Variability and trends of extreme temperature indices: (a) TX10p, (c) TN10p, and (e) CSDI. Spatial field of annual correlations between Sea Surface Temperature (SST) and (b) TX10p, (d) TN10p, and (f) CSDI for the period 1965–2013. HU, VH, and JCH station. ** Statistically significant trends at the 95% confidence level ($p < 0.05$). NCEP/NCAR Reanalysis. Source: NOAA/ESRL Physical Sciences Laboratory.

Overall, the oceanic influence on the extreme temperature indices in ML is very strong, modulated mainly by the increase/decrease of SST in the eastern and central Pacific. Figure 7b,d,f, and Figure 8a,b,e,f show that there are strong positive correlations ($+0.78 \leq r \leq +0.91$; $p < 0.05$) between SST in the Niño 1+2 region and the extreme tempera-

ture indices (TX90, TN90, WSDI, TXx, TXn, TNx, TNn, respectively). This suggests that the warming of SST in the Niño 1+2 region would cause an increase in TX90, TN90, TXx, TXn, TNx, TNn, and WSDI. Likewise, moderate and inverse associations were found between these extreme temperature indices and the SST in the northern and southern sectors of the western Pacific. The associations weaken with the Atlantic and Indian Oceans.

On the other hand, Figure 9b,d,f show that the associations between the extreme temperature indices (TX10, TN10, and CSDI), and the SSTs in Niño 1 + 2 region are moderate and inverse ($-0.69 \leq r \leq -0.44$; $p < 0.05$). Therefore, the SST cooling in Niño 1 + 2 region suggests an increase in TX10, TN10, and CSDI.

3.4.2. Extreme Precipitations

Overall, precipitation indices show a slight tendency toward wet conditions over ML since 1985. Figure 10a shows a significant decrease in the annual total wet-days precipitation (PRCPTOT), and the very wet days (R95p) at rates of -16 mm/decade and -5.3 mm/decade, respectively, during the 1970s. Then, both indices display an increasing trend toward wet conditions since 1985 ($+3.1$ mm/decade and $+1.4$ mm/decade, respectively). The highest values of PRCPTOT (30.7 mm) and R95p (16 mm) were recorded in 1970 due to the occurrence of the most extreme precipitation on 15 January 1970 (16 mm) in ML which is not attributable to the strong La Niña event of 1970. The most notorious influence of El Niño events on these indices was found during the years 1983, 2008, and 2009.

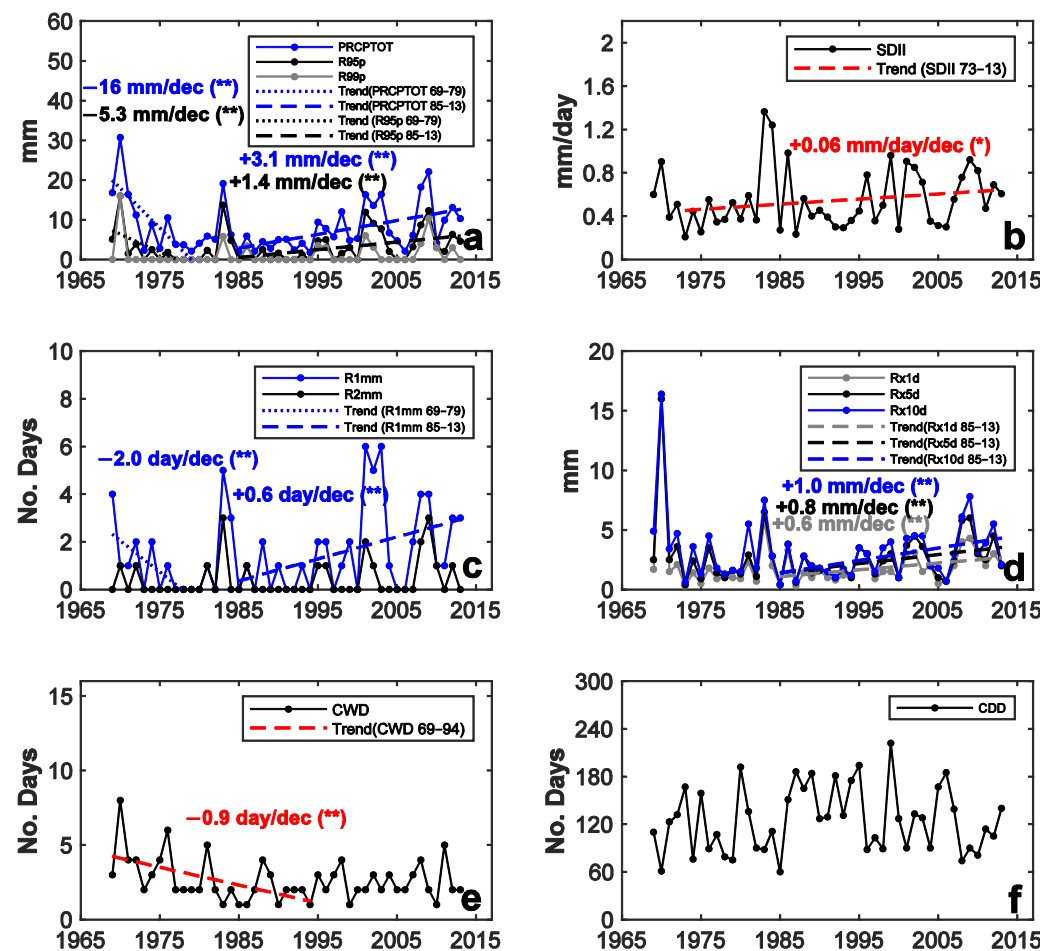


Figure 10. Linear trends of extreme precipitation indices: (a) PRCPTOT, R95p, R99p; (b) SDII; (c) R1mm, R2mm; (d) Rx1day, Rx5day, Rx10day; (e) CWD; and (f) CDD. PP > 0.1 mm were applied to identify a day with precipitation. HU station. ** Statistically significant trends at the 95% confidence level ($p < 0.05$). * Statistically significant trends at the 90% confidence level ($p < 0.10$).

Figure 10b illustrates the significant increasing trend (+0.06 mm/day/decade) in the simple daily intensity index of precipitation (SDII) during 1973–2013. The influence of the extraordinary El Niño event of 1983 on the daily intensity of precipitation is clear.

Heavy precipitation days over 10 mm (R10 mm) are unusual in ML; the most extreme case occurred on 15 January 1970 (16 mm). Usually, the precipitations in ML are less than 2 mm. Figure 10c shows a decrease of -2.0 days/decade in the number of days above 1 mm (R1 mm) during the 1970s, then an increase of +0.6 days/decade is observed during the period of 1985–2013. The number of days above 2 mm (R2 mm) shows no trend.

The maximum precipitation amount in 1, 5, and 10 consecutive days (Rx1day, Rx5day, Rx10day, respectively) increases significantly at rates of +0.6, +0.8, and +1.0 mm/decade, respectively during the period 1985–2013 (Figure 10d). In addition, it is observed that the maximum amounts in Rx1day, Rx5day, and Rx10day were registered in 1970 due to the occurrence of the most extreme precipitation on 15 January 1970 in ML. Moreover, the most notorious influence of El Niño events on these indices was found during the years 1983, 2008, and 2009.

Figure 10e shows a decrease of -0.9 days/decade in the consecutive wet days (CWD) during 1969–1994; after this period, there is no trend. A maximum of 8 consecutive wet days was recorded in July during La Niña event of 1970. On the other hand, Figure 10f shows no clear trend in the consecutive dry days (CDD) during 1969–2013.

In general, the influence of the Pacific Ocean SST on the extreme precipitation indices in ML is weak and variable in sign. However, precipitation is strongly altered during El Niño/La Niña episodes. Moreover, there could be other atmospheric mechanisms that would have a greater influence and require further investigation.

3.5. Extreme Precipitation Event of 15 January 1970, in ML

Table 3 shows the daily extreme precipitations that occurred in ML, and we can see that the most extreme event occurred on 15 January 1970. This event lasted about 5 h, from 18:00 to 23:00 h (Local Time—LT). The HU conventional station recorded 2 mm of precipitation until 18:00 LT on 15 January 1970, then 14 mm was recorded until 7:00 LT on 16 January 1970; therefore, the total accumulated precipitation was 16 mm corresponding to 15 January 1970 (LT).

Table 3. Date of occurrence of the daily extreme precipitations in ML (above the 99th percentile), HU station.

Year	Month	Day	mm
1970	1	15	16
1983	7	2	5.8
2009	7	20	4.3
2008	9	3	4
1995	12	26	3.5
1986	9	27	3.3
2002	2	5	3.1
1996	2	1	3
2001	2	4	3
2001	8	28	3
2009	11	28	3
2009	12	1	3
2010	1	7	3
2012	10	9	3

This extreme precipitation is not attributable to the strong La Niña event of 1970, due to the SST on the Peruvian coast beginning to decrease from April 1970 to November 1971; http://met.igp.gob.pe/elnino/lista_eventos.html (accessed on 28 June 2022). There are other atmospheric circulation conditions associated with this event, which will be analyzed in the following lines.

In the upper troposphere (200 hPa), Figure 11a,b displays the predominance of westerly winds over the Peruvian coasts in the days before the extreme precipitation event. However, on 15 January 1970, a change in the mean wind direction was observed (Figure 11c); the prevailing winds are from the east over the coastal zone of Lima (12° S). This change is caused by the intensification of the BH, which develops in the northern part of the Bolivian forest during this period and favors the passage of the warm and humid flows coming from the east (from the Amazonia) towards the central coast of the Peruvian territory. Easterly wind speeds are less than 10 m/s, enough to transport humidity towards the central coast of Peru. After the extreme precipitation event (Figure 11d), the westerly winds intensify slightly, favoring the incursion of flows from the Pacific Ocean.

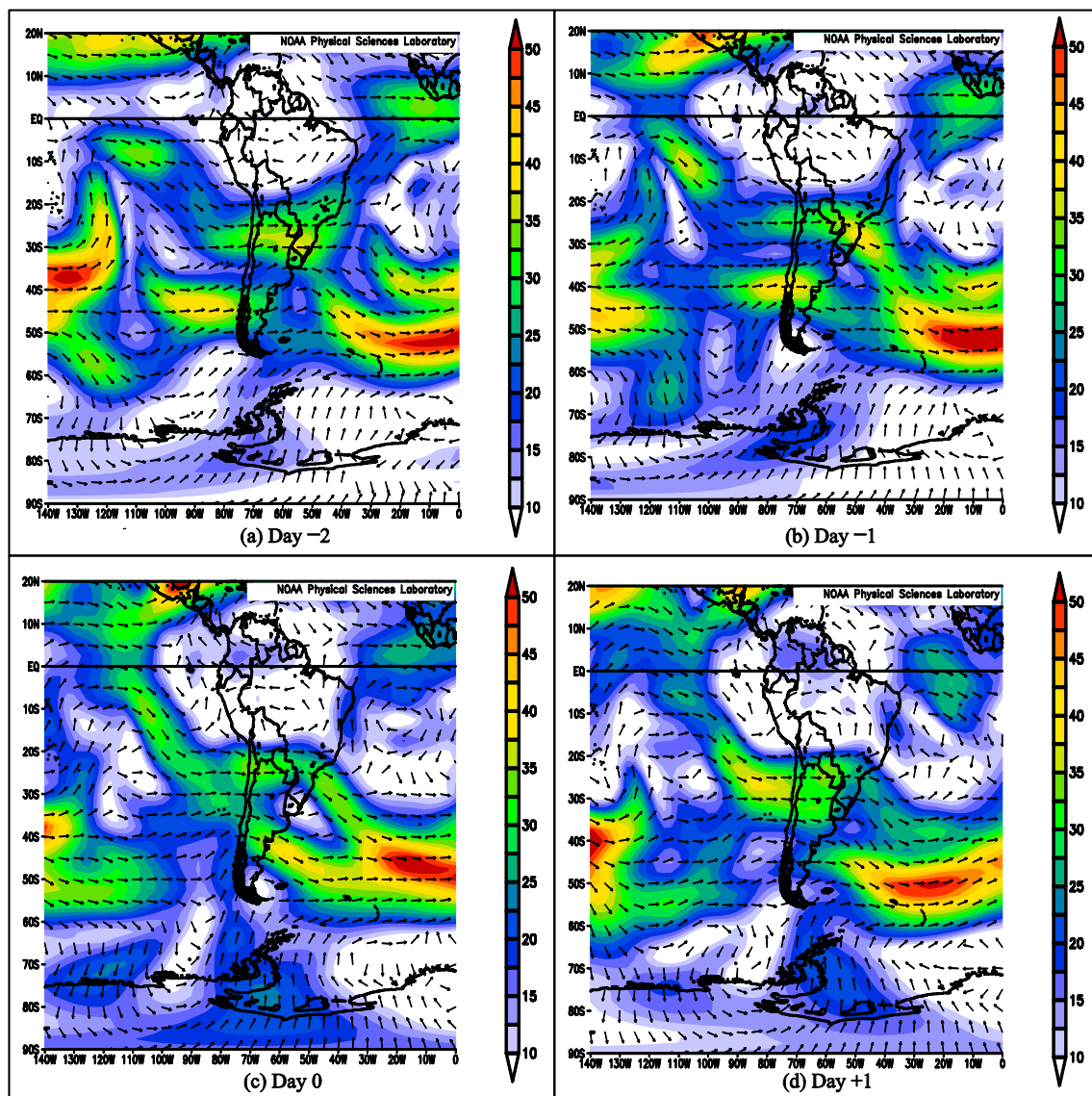


Figure 11. Wind composite mean (m/s) at high levels of the atmosphere (200 hPa) for (a) day -2, (b) day -1, (c) day 0, and (d) day +1 of the rainfall event on 15 January 1970. Source: NOAA/ESRL Physical Sciences Laboratory.

The analysis of wind anomalies at high levels of the atmosphere (200 hPa) shows an intense component from the west in the days before the event (Figure 12a,b). On the day of the event (Day 0), the intensity of the westerly wind anomalies decreased (Figure 12c), which explains the change in the mean wind direction from the west to the east in the

coastal region of Lima. This trend is maintained one day after the event (Figure 12d), these vectors have a slight inclination towards the north.

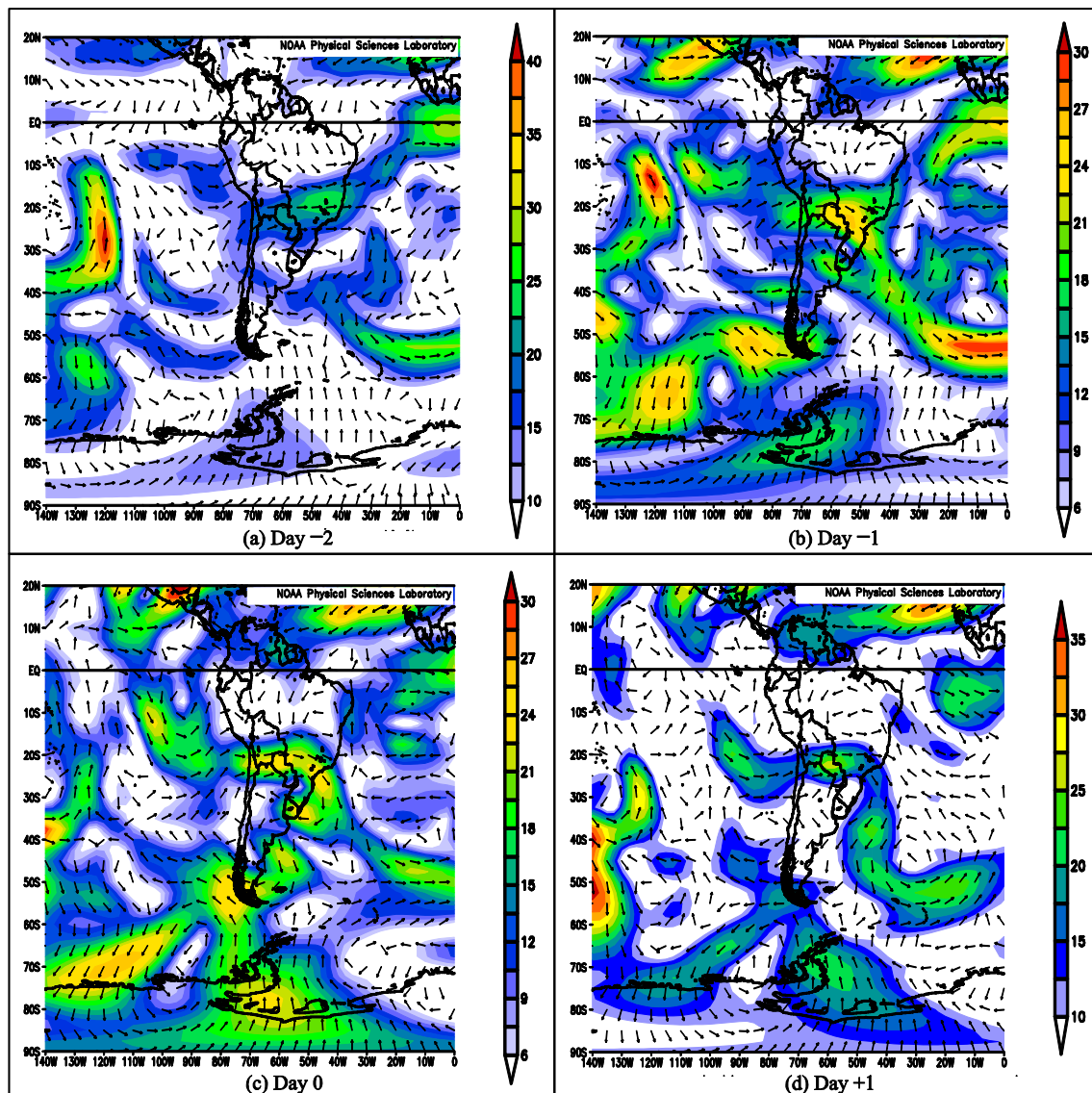


Figure 12. Wind composite anomaly (m/s) at high levels of the atmosphere (200 hPa) for (a) day -2 , (b) day -1 , (c) day 0, and (d) day $+1$ of the rainfall event on 15 January 1970. Source: NOAA/ESRL Physical Sciences Laboratory. The climatology base period is 1980–2010.

At mid levels of the atmosphere (500 Hpa), Figure 13a,b displays the intensification of the flows from the southeast in the Pacific in the days before the extreme precipitation event. On the day of the event and after it (Figure 13c,d), the southwest winds in the Pacific weaken; this allows the passage of wind-flow coming from the east and southeast towards the central coast over the mountain ranges of the Peruvian Andes, favoring the transportation of humid air masses from the Andes and the Amazon basin, which converge with the local circulation of ML, mainly in the afternoon.

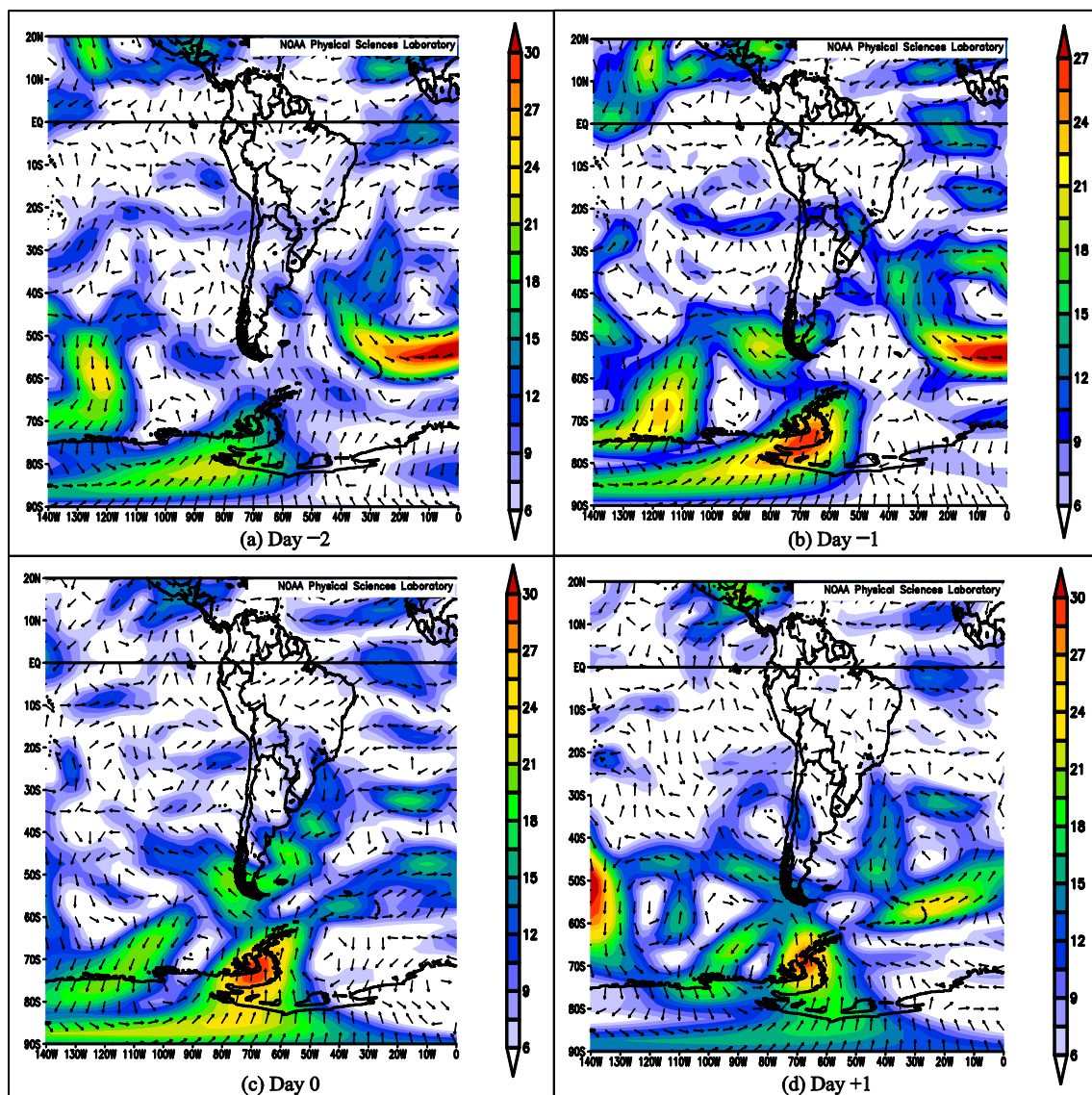


Figure 13. Wind composite anomaly (m/s) at mid levels of the atmosphere (500 hPa) for (a) day -2 , (b) day -1 , (c) day 0, and (d) day $+1$ of the rainfall event on 15 January 1970. Source: NOAA/ESRL Physical Sciences Laboratory. The climatology base period is 1980–2010.

At low levels of the atmosphere (850 Hpa), Figure 14a,b show the entry of northeasterly wind-flows into the coastal zone of Peru from the North Atlantic in the days before the extreme precipitation event; these northerly winds are deflected to the southwest by the effects of the Andes mountain range. Figure 14c,d show that northerly wind anomalies weaken over the entire central Peruvian Andes during the day of the extreme event and after it. On the other hand, Figure 14c shows the entry of westerly winds in a perpendicular direction to the coastal zone of Peru; this favors the incursion of hot and wet air masses coming from the sea at low levels, which combined with the humidity coming from mid and high levels of the atmosphere produced an increase in the instability of the atmosphere, causing very intense rains in ML.

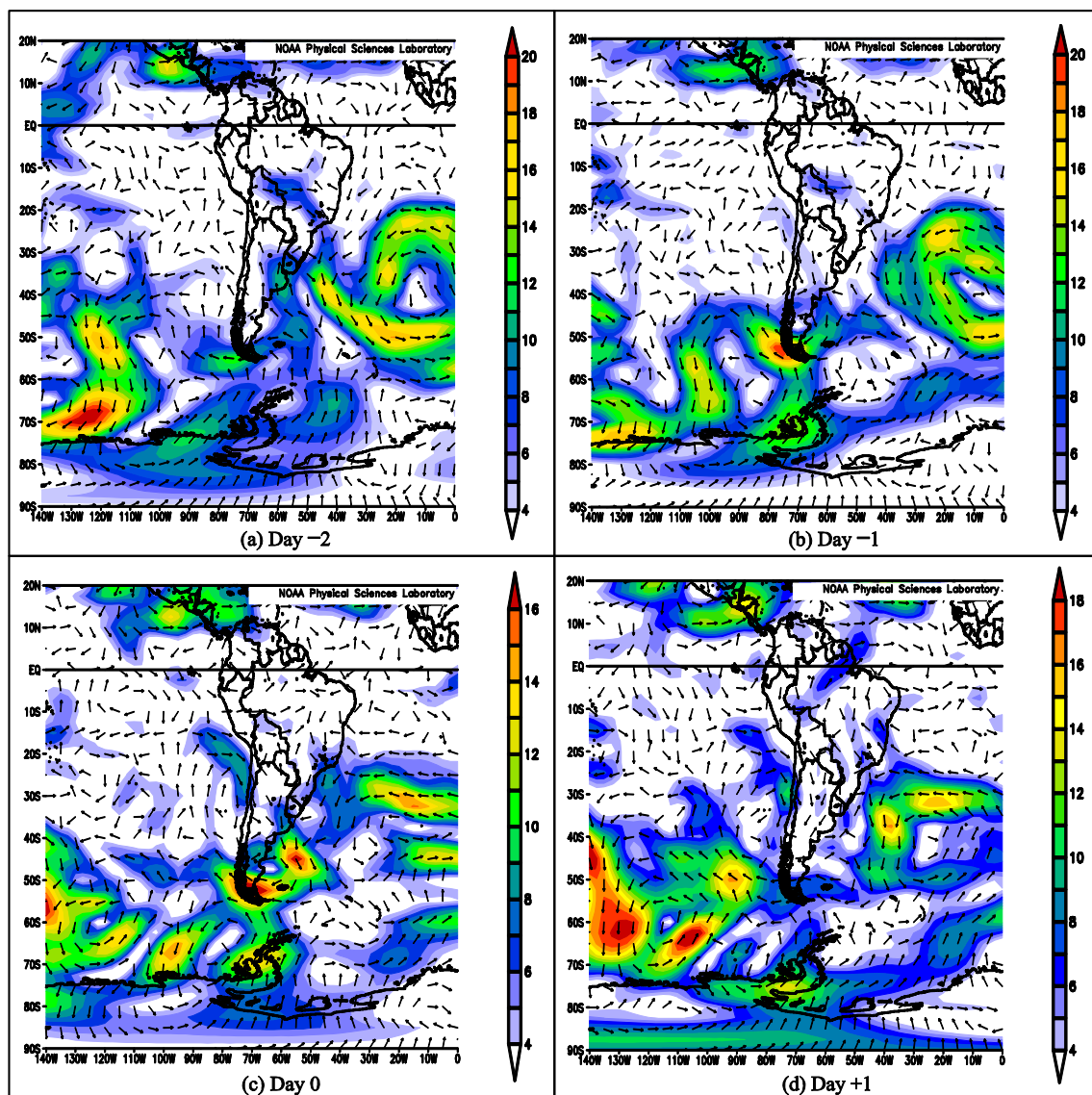


Figure 14. Wind composite anomaly (m/s) at low levels of the atmosphere (850 hPa) for (a) day -2 , (b) day -1 , (c) day 0, and (d) day $+1$ of the rainfall event on 15 January 1970. Source: NOAA/ESRL Physical Sciences Laboratory. The climatology base period is 1980–2010.

This incursion of air masses from the Pacific Ocean is reinforced by west wind anomalies at levels near the surface (925 hPa), these westerly winds were intensifying in regions near ML during the days before the event (Figure 15a,b). On the day of the event (Figure 15c), the western anomalies occur in a direction perpendicular to the Peruvian coastline, which favors the incursion of hot and humid air masses that cause the increase of atmospheric instability in the central coast regions of Peru. In addition, the start time of precipitation (18 LT) indicates the possibility that the sea breeze thermal circulation has intensified the transport of moist air masses from the ocean to the continent, triggering convection in regions close to ML [46]. The day after the event (Figure 15d), the wind vectors become parallel to the Peruvian coast, and the moist air-flows that come from the Pacific Ocean towards the continent decrease.

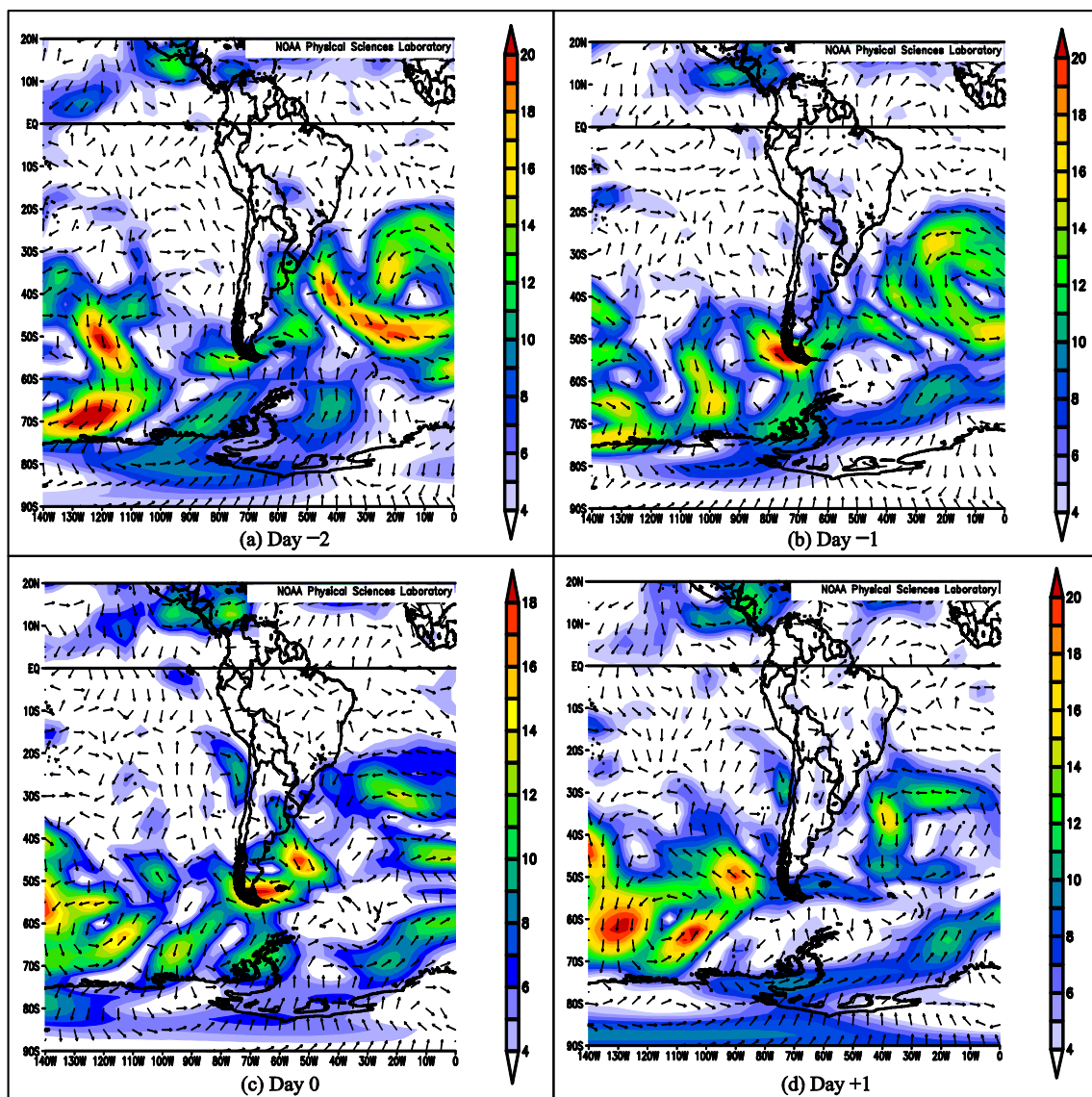


Figure 15. Wind composite anomaly (m/s) at near the surface of the atmosphere (925 hPa) for (a) day -2 , (b) day -1 , (c) day 0 , and (d) day $+1$ of the rainfall event on 15 January 1970. Source: NOAA/ESRL Physical Sciences Laboratory. The climatology base period is 1980–2010.

Figure 16a–c show the horizontal flow of the vertically integrated total column of water vapor flux (resolution: 2.5°) for the event of 15 January 1970, at 07, 13, and 19 LT, respectively. For all times, intense westerly moisture fluxes were observed at the west side of the Andes cordillera, perpendicular to the Peruvian coast, with values close to $300 \text{ kg m}^{-1} \text{ s}^{-1}$. Moreover, it is important to observe an intense moisture core located on the Pacific Ocean centered close to 20° S – 90° W , with values up to $1200 \text{ kg m}^{-1} \text{ s}^{-1}$. On the other hand, intense moisture fluxes were observed at the east side of the Andes (Amazon basin), related to the presence of the South America low-level jet (SALLJ), with values close to $100 \text{ kg m}^{-1} \text{ s}^{-1}$. It is likely that the convergence between these two moisture fluxes in regions close to the west side of the Andes cordillera caused the intense rainfall event in regions around the central Peruvian coast.

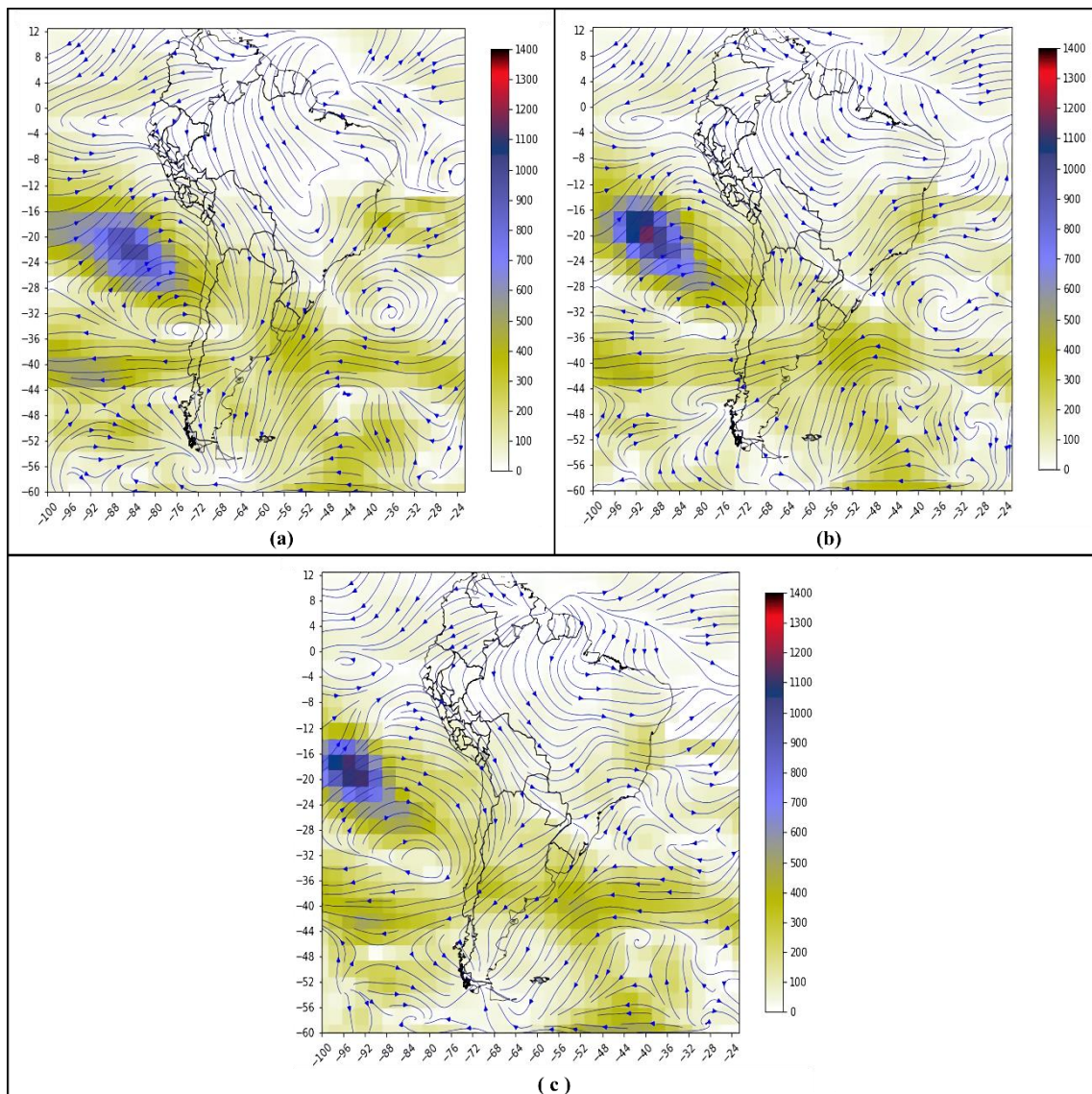


Figure 16. Horizontal vector flow of vertically integrated total column of water vapor flux ($\text{kg m}^{-1} \text{s}^{-1}$) during the rainfall event of 15 January 1970; calculated between 1000 hPa and 300 hPa for (a) 12 UTC (07 LT), (b) 18 UTC (13 LT), and (c) 00 UTC (19 LT). The geographic boundaries of South America and Peru are indicated. All fields were obtained from NCAR reanalysis data with 2.5-degree spatial resolution.

Presumably, the convergence between moisture fluxes coming from the east (Amazon region) at high (200 hPa) and mid levels (500 hPa), moisture fluxes coming from the west (Pacific Ocean) at low levels (850 hPa), and moisture fluxes near the surface (925 hPa) in the region close to the west side of the Andes cordillera caused the intense rainfall event in regions around the central Peruvian coast. It is important to highlight that these circulation patterns differ considerably from the climatic conditions (1981–2010) that prevail in the region.

4. Conclusions

The purpose of this work was to make a diagnosis of climate variability and extreme climate indices based on temperature and precipitation. In addition, the most extreme precipitation event that occurred in ML was analyzed. Based on the results and discussions presented in the previous section, we reach the following conclusions.

Thermal variations in the eastern tropical Pacific have a strong influence on the temperature in ML, in particular, the SST variability in Niño 1+2 region is closely linked to the temperature ($+0.90 \geq r \geq +0.85$; $p < 0.05$). Likewise, the extreme warm (cold) years are clearly associated with positive (negative) SST anomalies greater than $+0.5$ °C (lower than -0.5 °C) off the coasts of Peru and in the eastern tropical Pacific. In addition, westerly (easterly) wind anomalies towards the Peruvian central coast predominate at high levels of the atmosphere during extreme warm (cold) years. On the other hand, there is no clear association between rainfall in ML and SST variability in adjacent oceans; the atmospheric circulation has also been variable in the different levels of the atmosphere during extreme rainy (dry) years.

A thermal cooling trend was found in ML during the last two decades (1991–2013) at a rate of -0.5 °C/decade, which is consistent with the findings reported in other studies for coastal areas of central and southern Peru. This coastal cooling is probably due to the intensification of the winds along the coast, which is associated with coastal upwelling. On the other hand, PP has no trend during 1969–2013. However, PP had an increase of $+3.1$ mm/decade in ML during the last two decades (1991–2013).

There is a slight warming trend in extreme temperature indices (TXx, TNx, TXn, and TNn) in Lima during the period 1965–1998. However, the warming has not been constant; starting in 1999, there was a cooling trend, significantly in TXx (-1.0 °C/decade), which is consistent with the thermal cooling observed during the last two decades in ML.

Eastern tropical Pacific SSTs strongly influence the extreme temperature indices' variability. The associations between SST in the Niño 1+2 region and the indices (TX90, TN90, TXx, TXn, TNx, TNn, and WSDI) are strong and positive ($+0.78 \leq r \leq +0.91$; $p < 0.05$), while with the indices (TX10, TN10, and CSDI) are moderate and inverse ($-0.69 \leq r \leq -0.44$; $p < 0.05$). TX90, TN90, TXx, TXn, TNx, TNn, and WSDI increase but X10p, TN10p, and CSDI decrease during El Niño events; the opposite occurs during La Niña event.

The extreme precipitation indices indicate trends toward dry conditions during the 1970s. This trend reverses towards wet conditions after the 1980s. PRCTOT, R95p, SDII, R1mm Rx1day, Rx5day, and Rx10day show a significant increase of $+3.1$ mm/decade, $+1.4$ mm/decade, $+0.06$ mm/day/decade, $+0.6$ days/decade, $+0.6$ mm/decade, $+0.8$ mm/decade, and $+1.0$ mm/decade, respectively, during the period 1985–2013.

The atmospheric circulation analysis at high, mid, and low levels shows strong signs that the convergence between moisture fluxes from the east (Amazon region) at high and mid levels and the moisture fluxes from the west (Pacific Ocean) at low levels and near the surface caused the intense rainfall event in ML.

Author Contributions: Conceptualization, data collection, and analysis, L.G., G.T. and Y.S.; methodology, L.G. and Y.S.; elaboration of the figures and analysis of the results, L.G. and J.L.F.-R.; writing—original draft preparation, G.T., L.G. and Y.S.; writing—review and editing, L.G., Y.S. and J.L.F.-R.; supervision, Y.S. All authors have read and agreed to the published version of the manuscript.

Funding: This research was funded by Pontificia Universidad Católica del Perú, grant number CAP-2014.

Institutional Review Board Statement: Not applicable.

Informed Consent Statement: Not applicable.

Data Availability Statement: The data presented in this study are available on request from the corresponding author.

Acknowledgments: The authors thank The Pontifical Catholic University of Peru, The National Agrarian University La Molina, The Peruvian Corporation of Commercial Airports and Aviation, and The National Service of Meteorology and Hydrology of Peru for providing observed precipitation and temperature data. All authors thank reviewers for their very helpful contributions.

Conflicts of Interest: The authors declare no conflict of interest.

References

1. INEI. *Perú: Crecimiento y Distribución de La Población, 2017—Primeros Resultados*, 1st ed.; Instituto Nacional de Estadística e Informática: Lima, Perú, 2018. Available online: https://www.inei.gob.pe/media/MenuRecursivo/publicaciones_digitales/Est/Lib1530/libro.pdf (accessed on 13 May 2022).
2. Villacorta, S.; Nuñez, S.; Vasquez, J.; Pari, W.; Ochoa, M.; Benavente, C.; Tatard, L.; Luque, G.; Rosado, M.; Fidel, L.; et al. *Peligros Geológicos En El Area de Lima Metropolitana y La Region Callao*, 1st ed.; INGEMMET: Lima, Perú, 2015. Available online: <https://hdl.handle.net/20.500.12544/309> (accessed on 6 May 2022).
3. Villacorta, S.; De Torres, T.; Llorente, M.; Ayala, L.; Pérez-Puig, C.; Macharé, J.; Benavente, C. Datos Preliminares Sobre La Evolución Geomorfológica Del Abanico Aluvial de Lima, y Sus Implicaciones En El Análisis de Los Riesgos Asociados Al Cambio Climático. *Boletín La Soc. Geológica Del Perú* **2015**, *213*, 209–213. Available online: [App.ingemmet.gob.pe/biblioteca/pdf/BSGP-110-209.pdf](http://app.ingemmet.gob.pe/biblioteca/pdf/BSGP-110-209.pdf) (accessed on 3 April 2022).
4. Felix, M.L.; Kim, Y.K.; Choi, M.; Kim, J.C.; Do, X.K.; Nguyen, T.H.; Jung, K. Detailed Trend Analysis of Extreme Climate Indices in the Upper Geum River Basin. *Water* **2021**, *13*, 3171. [[CrossRef](#)]
5. Intergovernmental Panel on Climate Change (IPCC). *Climate Change 2013: The Physical Science Basis. Contribution of Working Group I to the Fifth Assessment Report of the Intergovernmental Panel on Climate Change*; Stocker, T.F., Qin, D., Plattner, G.-K., Tignor, S.K., Allen, J., Boschung, A., Nauels, Y., Xia, V.B., Midley, P.M., Eds.; Cambridge University Press: Cambridge, UK, 2013.
6. Donat, M.G.; Alexander, L.V.; Yang, H.; Durre, I.; Vose, R.; Dunn, R.J.H.; Willett, K.M.; Aguilar, E.; Brunet, M.; Caesar, J.; et al. Updated Analyses of Temperature and Precipitation Extreme Indices since the Beginning of the Twentieth Century: The HadEX2 Dataset. *J. Geophys. Res. Atmos.* **2013**, *118*, 2098–2118. [[CrossRef](#)]
7. Alexander, L.V.; Zhang, X.; Peterson, T.C.; Caesar, J.; Gleason, B.; Klein Tank, A.M.G.; Haylock, M.; Collins, D.; Trewin, B.; Rahimzadeh, F.; et al. Global Observed Changes in Daily Climate Extremes of Temperature and Precipitation. *J. Geophys. Res. Atmos.* **2006**, *111*, 1–22. [[CrossRef](#)]
8. Skansi, M.M.; Brunet, M.; Sigró, J.; Aguilar, E.; Arevalo Groening, J.A.; Bentancur, O.J.; Castellón Geier, Y.R.; Correa Amaya, R.L.; Jácome, H.; Malheiros Ramos, A.; et al. Warming and Wetting Signals Emerging from Analysis of Changes in Climate Extreme Indices over South America. *Glob. Planet. Change* **2013**, *100*, 295–307. [[CrossRef](#)]
9. Obregón, G.; Díaz, A.; Rosas, G.; Avalos, G.; Acuña, D.; Oria, C.; Llacza, A.; Miguel, R. *Second National Communication on Climate Change: Climate Scenarios for Peru to 2030*, 1st ed.; SENAMHI-PERÚ: Lima, Perú, 2009. Available online: https://www.ipcc.ch/apps/njlite/ar5wg2/njlite_download2.php?id=8834 (accessed on 13 April 2022).
10. SENAMHI. *Escenarios de Cambio Climático en la Cuenca del Río Mantaro Para el Año 2100: Resumen Técnico*, 1st ed.; Avalos, G., Dávila, J., Bracamonte, D., Galán, R., Eds.; Servicio Nacional de Meteorología e Hidrología (SENAMHI): Lima, Perú, 2009. Available online: https://www.senamhi.gob.pe/usr/cmn/pdf/PRAA_resu_tec_Escenarios_2100_MANTARO.pdf (accessed on 14 April 2022).
11. Huerta, A.; Lavado-Casimiro, W. Trends and Variability of Precipitation Extremes in the Peruvian Altiplano (1971–2013). *Int. J. Climatol.* **2021**, *41*, 513–528. [[CrossRef](#)]
12. De la Cruz Montalvo, G. *Escenarios Climáticos: Cambios en los Extremos Climáticos en el Perú Al 2050*, 1st ed.; SENAMHI-PERU: Lima, Peru, 2021. Available online: https://repositorio.senamhi.gob.pe/bitstream/handle/20.500.12542/1469/Escenarios-climaticos-cambios-en-los-extremos-climaticos-en-el-Peru-al-2050_2021.pdf?sequence=3&isAllowed=y (accessed on 2 April 2022).
13. El Comercio. Lima Sufre la Mayor Lluvia de los Últimos 45 años. Available online: <https://elcomercio.pe/bicentenario/1970-l-lima-sufre-la-mayor-lluvia-de-los-ultimos-45-anos-l-bicentenario-noticia/> (accessed on 25 January 2022).
14. Orrego Penagos, J.L. Lluvias históricas en Lima. Available online: <http://blog.pucp.edu.pe/blog/juanluisorrego/2010/03/30/lluvias-historicas-en-lima/> (accessed on 14 February 2022).
15. Caretas. Así Fue el insólito Diluvio que Azotó Lima hace 50 años. Available online: <https://caretas.pe/nacional/asi-fue-el-insolito-diluvio-que-azoto-lima-hace-50-anos-lluvia-torrencial-inundacion-50-anos-efemerides-callao/> (accessed on 12 April 2022).
16. Sanabria, J.; Bourrel, L.; Dewitte, B.; Frappart, F.; Rau, P.; Solis, O.; Labat, D. Rainfall along the coast of Peru during Strong El Niño Events. *Int. J. Climatol.* **2018**, *38*, 1737–1747. [[CrossRef](#)]
17. Takahashi, K.; Martínez, A.G. The Very Strong Coastal El Niño in 1925 in the Far-Eastern Pacific. *Clim. Dyn.* **2017**, *52*, 7389–7415. [[CrossRef](#)]
18. Christensen, J.H.; Krishna Kumar, K.; Aldrian, E.; An, S.-I.; Cavalcanti, I.F.A.; de Castro, M.; Dong, W.; Goswami, P.; Hall, A.; Kanyanga, J.K.; et al. Climate Phenomena and Their Relevance for Future Regional Climate Change. In *Climate Change 2013: The Physical Science Basis. Contribution of Working Group I to the Fifth Assessment Report of the Intergovernmental Panel on Climate Change*; Stocker, T.F., Qin, D., Plattner, G.-K., Tignor, M., Allen, S.K., Boschung, J., Nauels, A., Xia, Y., Bex, V., Midley, P.M., Eds.; Cambridge University Press: Cambridge, UK; New York, NY, USA, 2013. [[CrossRef](#)]
19. INEI. *Conociendo Lima: Guía Estadística*, 1st ed.; Dirección Nacional de Estadística e Informática Departamental, Ed.; Dirección Nacional de Estadística e Informática Departamental: Lima, Perú, 2001. Available online: https://www.inei.gob.pe/media/MenuRecursivo/publicaciones_digitales/Est/Lib0410/Libro.pdf (accessed on 12 April 2022).
20. Siña, M.; Wood, R.C.; Saldarriaga, E.; Lawler, J.; Zunt, J.; Garcia, P.; Cárcamo, C. Understanding Perceptions of Climate Change, Priorities, and Decision-Making among Municipalities in Lima, Peru to Better Inform Adaptation and Mitigation Planning. *PLoS ONE* **2016**, *11*, e0147201. [[CrossRef](#)]

21. Miranda Sara, L.; Jameson, S.; Pfeffer, K.; Baud, I. Risk Perception: The Social Construction of Spatial Knowledge around Climate Change-Related Scenarios in Lima. *Habitat Int.* **2016**, *54*, 136–149. [CrossRef]
22. Capel, J.J. Lima, Un Clima de Desierto Litoral. *An. Geogr. Univ. Complut.* **1999**, *19*, 25–45. Available online: <https://dialnet.unirioja.es/servlet/articulo?codigo=86529> (accessed on 16 May 2022).
23. Rivas, P. Identificación de patrones de circulación característicos en la formación de precipitación en Lima Metropolitana y Callao durante 1980–1995. Tesis para optar el título profesional de Ingeniero Meteorólogo, Universidad Nacional Agraria La Molina (UNALM), Lima, Perú, 2019. Available online: <https://hdl.handle.net/20.500.12996/4227> (accessed on 5 June 2022).
24. Castro, A.; Davila, C.; Will, L.; Cubas, F.; Avalos, G.; Lopez, C.; Villena, D.; Valdez, M.; Urbiola, J.; Trebejo, I.; et al. *Climas Del Perú-Mapa de Clasificación Climática Nacional*, 1st ed.; SENAMHI-Perú: Lima, Perú, 2020. Available online: <https://www.senamhi.gob.pe/load/file/01404SENA-4.pdf> (accessed on 3 June 2022).
25. Hanley, D.E.; Bourassa, M.A.; O'Brien, J.J.; Smith, S.R.; Spade, E.R. A Quantitative Evaluation of ENSO Indices. *J. Clim.* **2003**, *16*, 1249–1258. [CrossRef]
26. Trenberth, K.E. The Definition of El Niño. *Bull. Am. Meteorol. Soc.* **1997**, *74*, 2771–2778. [CrossRef]
27. Trenberth, K.; National Center for Atmospheric Research. The Climate Data Guide: Nino SST Indices (Nino 1+2, 3, 3.4, 4; ONI and TNI). Available online: <https://climatedataguide.ucar.edu/climate-data/nino-sst-indices-nino-12-3-34-4-oni-and-tni> (accessed on 26 March 2022).
28. Kalnay, E.; Kanamitsu, M.; Kistler, R.; Collins, W.; Deaven, D.; Gandin, L.; Iredell, M.; Saha, S.; White, G.; Woollen, J.; et al. The NCEP/NCAR 40-Year Reanalysis Project. *Bull. Am. Meteorol. Soc.* **1996**, *77*, 437–471. [CrossRef]
29. Zhang, X.; Feng, Y.; Chan, R. *Introduction to RCLimDex v1.9*; Climate Research Division Environment Canada: Downsview, ON, Canada, 2018. Available online: <https://usermanual.wiki/Document/manual.2056401896.pdf> (accessed on 11 June 2022).
30. Aswad, F.K.; Yousif, A.A.; Ibrahim, S.A. Trend Analysis Using Mann-Kendall Snd Sen's Slope Estimator Test for Annual and Monthly Rainfall for Sinjar District, Iraq. *J. Univ. Duhok* **2020**, *23*, 501–508. Available online: <https://journal.uod.ac/index.php/uodjournal/article/view/954/686> (accessed on 14 May 2022). [CrossRef]
31. Alfaro, L. *Estimación de Umbrales de Precipitaciones Extremas Para La Emisión de Avisos Meteorológicos*; Nota Técnica: Lima, Perú, 2014. Available online: <https://www.senamhi.gob.pe/load/file/01402SENA-6.pdf> (accessed on 14 June 2022).
32. Mann, H.B. Nonparametric Tests Against Trend. *Econometrica* **1945**, *13*, 245–259. [CrossRef]
33. Kendall, M.G. *Rank Correlation Methods*, 4th ed.; Charles Griffin: London, UK, 1975.
34. Sen, P.K. Estimates of the Regression Coefficient Based on Kendall's Tau. *J. Am. Stat. Assoc.* **1968**, *63*, 1379–1389. [CrossRef]
35. Hirsch, R.M.; Slack, J.R.; Smith, R.A. Techniques of Trend Analysis for Monthly Water Quality Data. *Water Resour. Res.* **1982**, *18*, 107–121. [CrossRef]
36. Gocic, M.; Trajkovic, S. Analysis of Changes in Meteorological Variables Using Mann-Kendall and Sen's Slope Estimator Statistical Tests in Serbia. *Glob. Planet. Chang.* **2013**, *100*, 172–182. [CrossRef]
37. Hernández-Lalinde, J.D.; Espinosa-Castro, J.F.; Peñalosa-Tarazona, M.E.; Rodriguez, J.E.; Chacón-Rangel, J.G.; Toloza-Sierra, C.A.; Arenas-Torrado, M.K.; Carrillo-Sierra, S.M.; Bermúdez-Pirela, V.J. Sobre El Uso Adecuado Del Coeficiente de Correlación de Pearson: Definición, Propiedades y Suposiciones. *AVFT-Arch. Venez. Farmacol. Ter.* **2018**, *37*, 587–595. Available online: https://www.revistaavft.com/images/revistas/2018/avft_5_2018/25sobre_uso_adequado_coeficiente.pdf (accessed on 11 May 2022).
38. Rodgers, J.L.; Nicewander, A.W. Thirteen Ways to Look at the Correlation Coefficient. *Am. Stat. Assoc.* **1988**, *42*, 59–66. [CrossRef]
39. Zhang, X.; Alexander, L.; Hegerl, G.C.; Jones, P.; Klein Tank, A.; Peterson, T.C.; Trewin, B.; Zwiers, F.W. Indices for Monitoring Changes in Extremes Based on Daily Temperature and Precipitation Data. *Wiley Interdiscip. Rev. Clim. Chang.* **2011**, *2*, 851–870. [CrossRef]
40. Klein Tank, A.M.G.; Zwiers, F.W.; Zhang, X. *Guidelines on Analysis of Extremes in a Changing Climate in Support of Informed Decisions for Adaptation*; WMO: Geneva, Switzerland, 2009. Available online: https://www.ecad.eu/documents/WCDMP_72_TD_1500_en_1.pdf (accessed on 17 January 2022).
41. Peterson, T.C.; Folland, C.; Gruza, G.; Hogg, W.; Mokssit, A.; Plummer, N. *Report on the Activities of the Working Group on Climate Change Detection and Related Rapporteurs 1998-2001*; World Meteorological Organization: Geneva, Switzerland, 2001. Available online: http://www.clivar.org/sites/default/files/documents/048_wgccd.pdf (accessed on 23 January 2022).
42. Karl, T.; Nicholls, N.; Ghazi, A. CLIVAR/GCOS/WMO Workshop on Indices and Indicators for Climate Extremes. In *Climate Change*; Kluwer Academic Publishers: Dordrecht, Netherlands, 1999; Volume 42, pp. 3–7. Available online: https://link.springer.com/chapter/10.1007/978-94-015-9265-9_2 (accessed on 22 January 2022).
43. Gutiérrez, D.; Bouloubassi, I.; Sifeddine, A.; Purca, S.; Goubanova, K.; Graco, M.; Field, D.; Méjanelle, L.; Velazco, F.; Lorre, A.; et al. Coastal Cooling and Increased Productivity in the Main Upwelling Zone off Peru since the Mid-Twentieth Century. *Geophys. Res. Lett.* **2011**, *38*, 1–6. [CrossRef]
44. Gutiérrez, D.; Bertrand, A.; Wosnitza-Mendo, C.; Dewitte, B.; Purca, S.; Peña, C.; Chaigneau, A.; Tam, J.; Graco, M.; Echevin, V.; et al. Climate Change Sensitivity of the Peruvian Upwelling System and Ecological Implications. *Rev. Peru. Geo-Atmosférica* **2011**, *26*, 1–26. Available online: https://horizon.documentation.ird.fr/exl-doc/pleins_textes/2021-08/010082418.pdf (accessed on 29 June 2022).

45. Falvey, M.; Garreaud, R.D. Regional Cooling in a Warming World: Recent Temperature Trends in the Southeast Pacific and along the West Coast of Subtropical South America (1979–2006). *J. Geophys. Res.* **2009**, *114*, D04102. [[CrossRef](#)]
46. Flores-Rojas, J.L.; Moya-Álvarez, A.S.; Valdivia-Prado, J.M.; Piñas-Laura, M.; Kumar, S.; Karam, H.A.; Villalobos-Puma, E.; Martínez-Castro, D.; Silva, Y. On the Dynamic Mechanisms of Intense Rainfall Events in the Central Andes of Peru, Mantaro Valley. *Atmos. Res.* **2021**, *248*, 105188. [[CrossRef](#)]